


# Wave Analysis and Homogenization of a Spatiotemporally Modulated Wire Medium

Michael Kreiczler and Yakir Hadad<sup>\*</sup>

*School of Electrical Engineering, Tel Aviv University, 69978 Ramat-Aviv, Israel*

 (Received 7 June 2021; revised 29 September 2021; accepted 8 October 2021; published 2 November 2021)

We develop a homogenization theory for a spatiotemporally modulated wire medium. We first solve for the modal waves that are supported by this composite medium, and we show peculiar properties such as extraordinary waves that propagate at frequencies below the cutoff frequency of the corresponding stationary medium. We explain how these unique solutions give rise to an extreme Fresnel drag that exists already with weak and slow spatiotemporal modulation. Next we derive the effective material permittivity that corresponds to each of the first few supported modes, and write the average fields and Poynting vector. Nonlocality, nonreciprocity, and anisotropy due to the spatiotemporal modulation are three inherent properties of this medium, and are clearly seen in the effective material parameters. Lastly, we validate that homogenization and spatiotemporal variation are not necessarily interchangeable operations. Indeed, in certain parameter regimes the homogenization should be performed directly on the spatiotemporally modulated composite medium, rather than the stationary medium being homogenized first and then the effect of the space-time modulation being introduced phenomenologically.

DOI: [10.1103/PhysRevApplied.16.054003](https://doi.org/10.1103/PhysRevApplied.16.054003)

## I. INTRODUCTION

The study of electromagnetic wave dynamics in time-varying media goes back several decades [1,2]. Recently, there has been renewed interest in research in this direction, especially in the context of new developments toward the next generation of metamaterials [3–16], including devices that outperform physical linear-time-invariant (LTI) bounds [17–21]. Such progress is accompanied by new technological abilities that make the actual realization of engineered time-varying media plausible.

Most recent studies on time-varying media have explored wave phenomena and potential applications where the time modulation was considered by assuming certain, given, time-varying effective constitutive relations, such as effective permittivity, permeability, and conductivity. However, such a medium will typically be implemented as a metamaterial. This raises the question of the correct modeling of such a *composite* medium, and specifically, the connections between its microstructure time-varying properties and its macroscopic effective medium characteristics. In this paper, we address these issues for the specific case of a spatiotemporally modulated, capacitively loaded, infinite wire medium (see Fig. 1).

Despite its apparent simplicity that allows relatively-easy-to-follow analytical modeling, the wire medium, even in its simplest two-dimensional lattice form, gives rise to various peculiar properties, such as strong anisotropy,

effective plasmlike dispersion, and strong nonlocality [22–38]. Therefore, it is a particularly interesting platform to use to explore wave phenomena and homogenization when one is considering the time modulation already at the microscopic meta-atom level.

In this work our goal is twofold. First, taking into account the *complete interaction* between spatiotemporally modulated loaded wires (meta-atoms), we explore the various wave phenomena that can be supported by this medium. Particularly, we study (i) nonreciprocal and anisotropic propagation due to the spatiotemporal modulation, (ii) the existence of extraordinary waves that propagate at frequencies that are below the so-called plasma frequency of the stationary wire medium (i.e., in the absence of modulation), even with a negligible modulation index, and thus that are akin to the whistler mode in magnetized plasma [39], and consequently (iii) the emergence of Fresnel drag [40] already with weak and slow modulation. Second, we aim to derive effective medium properties when the meta-atoms are time modulated. In particular we explore the effect of taking into account the time modulation already in the homogenization process, as opposed to first homogenizing the stationary medium and later introducing the time modulation into the effective properties. Put differently, we try to address the effect of the spatiotemporal modulation on the homogenization. Related to that is the issue of dispersion in the presence of time modulation; this was recently tackled in several studies, such as Refs. [41,42]. Here we study the specific wire-medium case using a quasi-frequency-domain approach, and take

<sup>\*</sup>hadady@eng.tau.ac.il

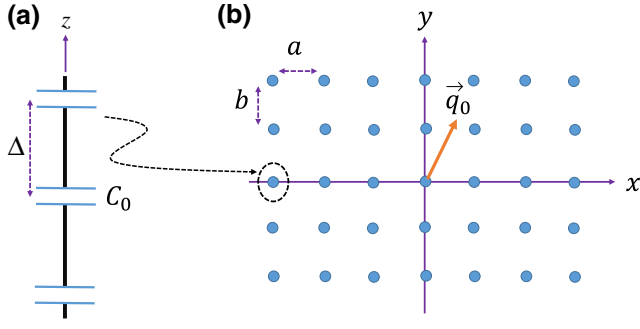


FIG. 1. (a) Capacitively loaded wire. (b) The wire medium on a rectangular lattice with unit-cell dimensions  $a$  along  $x$  and  $b$  along  $y$ . In this work we focus on waves that propagate transversely to the wires with  $\vec{q} = q_x \hat{x} + q_y \hat{y}$ .

the complete interwire interaction that comprises the composite medium, as discussed below. We pay particular attention to the wave dynamics near the plasma frequency, where, because of the sensitivity of the zero-crossing point of the effective transverse permittivity of the stationary wire medium, interesting phenomena occur as soon as we introduce weak spatiotemporal modulation.

The paper is organized as follow. For completeness, in Sec. II, we begin with a brief review of stationary capacitively loaded wire media. Then, in Sec. III we introduce spatiotemporal modulation to the capacitive loads and provide a through mathematical formulation to solve the modal problem. In Sec. IV, focusing on a narrow frequency range near the plasma frequency of the corresponding stationary lattice, we derive analytical expressions for the dispersion relations of the first lowest-order modes supported in the lattice, and study the wave dynamics in this parameter domain. In Sec. V, we derive the effective medium parameters of several supported modes; in addition, we derive expressions for the averaged electric and magnetic fields, and the corresponding Poynting vector in this case. In Sec. VI we explore numerically the excitation dynamics of a finite, spatiotemporally modulated, wire-medium sample. Finally, in Sec. VII, we compare the wave phenomena in the time-modulated wire medium and the wave phenomena predicted when the time modulation is introduced into the effective medium properties of the stationary wire medium (i.e., after homogenization).

## II. STATIONARY CAPACITIVELY LOADED WIRE MEDIUM

In the following sections we analyze wave phenomena in spatiotemporally modulated loaded-wire media. Unavoidably, we frequently refer to the derivation and the main results for the corresponding stationary case. Therefore, to make the paper self-contained, in this section we briefly review a *stationary* capacitively loaded wire medium. We mainly follow the analysis in Ref. [38] for

general wire loading, and stress the more-relevant aspects for the spatiotemporal problem to follow.

Assume that a  $\hat{z}$ -polarized electromagnetic wave is propagating inside an infinite loaded wire medium as shown in Fig. 1. We assume that the wires are surrounded by a vacuum with permittivity  $\epsilon_0$  and permeability  $\mu_0$ . The lattice points are given by  $R_{m,l} = ma\hat{x} + lb\hat{y}$ , where  $a$  and  $b$  are the unit-cell dimensions and  $m$  and  $l$  denote the unit-cell indices. The induced current in each of the wires is given by  $\vec{I} = \alpha \vec{E}^{\text{loc}}$ , where  $\vec{E}^{\text{loc}}$  is the local electric field (namely, the electric field at the wire location but in the absence of the wire itself) and  $\alpha$  is the wire's susceptibility. If the wires are periodically loaded by lumped impedance  $Z_L$  with periodicity  $\Delta \ll \lambda$ , the inverse susceptibility is given by [38]

$$\alpha^{-1}(\omega) = \alpha_0^{-1}(\omega) + \frac{Z_L}{\Delta}, \quad (1)$$

where  $\alpha_0^{-1}(\omega) = (\eta k/4)H_0^{(2)}(kr_0)$ . For serial loading of lumped capacitors  $Z_L/\Delta = 1/j\omega\tilde{C}_0$  and  $\tilde{C}_0 = C_0\Delta$ . Here  $\eta = 120\pi\Omega$  and  $k = \omega/c$  are the free-space impedance and wave number, respectively,  $\omega$  is the radial frequency,  $c$  is the speed of light in a vacuum,  $r_0$  is the wire radius, and  $H_0^{(2)}$  denotes the zero-order Hankel function of the second kind. There are additional, more-accurate ways to describe the periodic wire loading [43,44]; however, since we consider mainly the fundamental physical effects, we limit this work to the relatively simple and intuitive approximation in Eq. (1), which has been demonstrated to be effective and sufficiently accurate through full-wave simulations and experiments in various studies [45,46]. In light of the lattice periodicity, the Floquet-Bloch wave solution as follows:

$$I_{m,l} = I_0 e^{-j(q_x am + q_y bl)}, \quad (2)$$

where  $q_x$  and  $q_y$  stand for the transverse (with respect to  $z$ ) components of the wave number in the wire medium. Throughout this paper we assume for simplicity that  $q_z = 0$ , which is in accord with our initial assumption that the electric field is polarized solely along  $z$ . Under the assumptions above, the wave-number dispersion is found by solving

$$E_z^{\text{loc}}(I_0) = \alpha^{-1}(\omega)I_0, \quad (3)$$

where  $E_z^{\text{loc}}$  denotes the local field acting on the wire (See Appendix A) at  $m = l = 0$ . Following Ref. [38] it is given by

$$E_z^{\text{loc}} = -I_0 \frac{\eta k}{2} \left( S_0 + \sum_{m \neq 0} S_m e^{-jq_x am} \right), \quad (4)$$

with

$$S_0 = \sum_{l=1}^{\infty} H_0^{(2)}(kR_{0l}) \cos q_y b l \quad (5a)$$

$$S_m = \frac{1}{2} \sum_{l=-\infty}^{\infty} H_0^{(2)}(kR_{ml}) e^{-j q_y b l}, \quad (5b)$$

where  $R_{ml} = \sqrt{(ma)^2 + (lb)^2}$ . The infinite slowly converging series in Eqs. (5a) and (5b) may be converted into fast converging series using for example, Poisson summation [38,47]. For a dense grid,  $ka, kb \ll 1$ , the dispersion relation may be approximated by

$$\omega \tilde{L}_w - \frac{1}{\omega \tilde{C}_0} = \frac{k\eta}{ab(k^2 - q^2)}, \quad (6)$$

where  $q^2 = q_x^2 + q_y^2$  and

$$\tilde{L}_w = \frac{\eta}{2c} \left( \frac{1}{\pi} \ln \frac{b}{2\pi r_0} + \sum_{l=1}^{\infty} \frac{\coth(\pi a l/b) - 1}{\pi l} + \frac{a}{6b} \right), \quad (7)$$

which denotes the per-unit-length intrinsic wire inductance. For the dense-grid case, the dispersion equation depends only on  $q = \sqrt{q_x^2 + q_y^2}$ . Then, an equation for the effective permittivity along the longitudinal (with respect to  $z$ ) axis is obtained as  $\varepsilon_z = q^2/k^2$ . This yields

$$\varepsilon_z(\omega) = \varepsilon_0 \left( 1 - \frac{k_p^2(k)}{k^2} \right), \quad (8)$$

with

$$k_p^2(k) = \frac{\eta k}{ab(\omega \tilde{L}_w - 1/\omega \tilde{C}_0)} \quad (9)$$

and  $k = \omega/c$ . Here and henceforth,  $k_p$  is the plasma frequency. Nevertheless, unlike unloaded wire media, for which effectively  $\tilde{C}_0 \rightarrow \infty$  and consequently  $k_p^2 = (\eta/c)/ab\tilde{L}_w = (1/\tilde{C}_b\tilde{L}_w)/c^2$ , where  $\tilde{C}_b = ab\varepsilon_0$  is frequency independent, when the wires are loaded the behavior is not that of a typical plasma since  $k_p$  depends on  $k$ . In the following,  $\tilde{C}_b$  is the per-unit-length background capacitance.

### III. WIRE MEDIA WITH SPATIOTEMPORALLY MODULATED CAPACITIVE LOADING

Our first goal is to study wave propagation in spatiotemporally modulated wire media (see illustration in Fig. 2). To that end, we generalize the conventional approach for

stationary LTI wire media described above. Our analysis is based on the concept of harmonic balance that can be regarded as a quasi-frequency-domain technique. In this sense, our method is less general than, for example, that in Ref. [48], which suggests, in principle, a direct time-domain approach to that problem. However, since we focus on the particular case of small time-harmonic capacitance perturbation, we find this method, as discussed below, to be more direct and therefore a better fit for this problem.

#### A. The response of a single wire

Consider the periodically loaded and time-modulated wire in Fig. 2a. Assume that the loading capacitance on each of the wires is modulated as

$$C(t) = C_0 + \delta C \cos(\Omega t - \varphi), \quad m = \frac{\delta C}{C_0} \ll 1. \quad (10)$$

Here and henceforth,  $\Omega$  denotes the modulation frequency,  $m$  denotes the modulation depth, and  $\varphi$  is an additional phase term that will enable the effective spatiotemporal modulation by enforcing certain phase differences between the wires. In the absence of time modulation, the time-domain counterpart of Eq. (3) is given by  $\widehat{E}^{\text{loc}}(t) = \widehat{\alpha}^{-1}(t) * \widehat{I}(t)$ , where ‘‘wide-hat’’  $\widehat{X}(t)$  represents the time-domain, inverse-Fourier-transform counterpart of  $X(\omega)$ , where  $X$  stands for either  $E^{\text{loc}}$ ,  $\alpha^{-1}$ , or  $I$ . This time-domain perspective enables us to naturally introduce the effect of the time modulation on the capacitors (see Appendix B):

$$\widehat{E}^{\text{loc}}(t) = \widehat{\alpha}_0^{-1}(t) * \widehat{I}(t) + \frac{1}{\tilde{C}(t)} \int_{-\infty}^t I(\tau) d\tau, \quad (11)$$

with  $\tilde{C}(t) = C(t)\Delta$ . By using  $1/(1+x) \approx 1-x$  for  $x \ll 1$ , by inserting Eq. (10) in Eq. (11), and by transformation

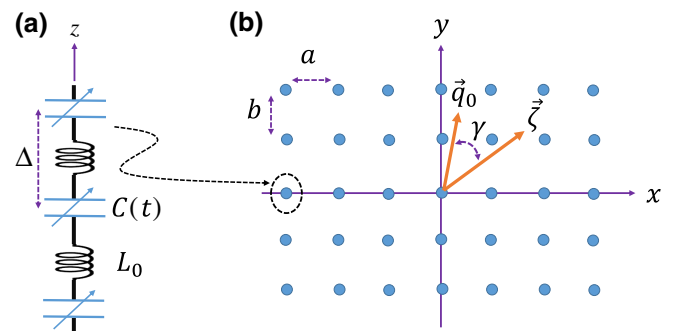


FIG. 2. (a) The time-modulated loaded wire.  $L_0$  increases the self-inductance of the wire, and  $C(t)$  introduces the time-modulated capacitance. These lumped elements are periodically loaded on the wire with periodicity  $\Delta$ , thus creating the effective wire time-modulated susceptibility. (b) The wire medium. Each wire is modulated with the same temporal frequency  $\Omega$  but with a different phase that is determined by the modulation wave vector  $\zeta$ . The propagation occurs with fundamental wave vector  $\vec{q}_0$ .

to the frequency domain, we get

$$E^{\text{loc}}(\omega) = \left( \alpha_0^{-1}(\omega) + \frac{1}{j\omega\tilde{C}_0} \right) I(\omega) - \frac{m}{2} \left( \frac{e^{-j\varphi}}{j(\omega - \Omega)\tilde{C}_0} I(\omega - \Omega) + \frac{e^{j\varphi}}{j(\omega + \Omega)\tilde{C}_0} I(\omega + \Omega) \right). \quad (12)$$

Consider now a particular nominal frequency  $\omega_0$ , which may be, for instance, the excitation frequency of a monochromatic impinging wave or the excitation frequency of a localized source within the bulk. Then, in light of the harmonic time modulation, the local field has the following frequency dependence:

$$E^{\text{loc}}(\omega) = \sum_{n=-\infty}^{\infty} E_n^{\text{loc}} \delta(\omega - \omega_n), \quad (13)$$

where  $\omega_n = \omega_0 + n\Omega$  and where  $\delta(\cdot)$  denotes Dirac's  $\delta$ . Then, for the current we have

$$I(\omega) = \sum_{n=-\infty}^{\infty} I_n \delta(\omega - \omega_n), \quad (14)$$

where  $E_n^{\text{loc}}$  and  $I_n$  denote the  $n$ th-harmonic amplitude of the local field and the induced current, respectively. By plugging Eqs. (13) and (14) into Eq. (12) and by balancing the coefficients of equal harmonics, we find

$$E_n^{\text{loc}} = \left( \alpha_0^{-1}(\omega_n) + \frac{1}{j\omega_n\tilde{C}_0} \right) I_n - \frac{m}{2} \left( \frac{e^{-j\varphi}}{j\omega_{n-1}\tilde{C}_0} I_{n-1} + \frac{e^{j\varphi}}{j\omega_{n+1}\tilde{C}_0} I_{n+1} \right). \quad (15)$$

## B. The time-modulated lattice

Our goal is to analyze a spatiotemporally modulated wire medium (as illustrated in Fig. 2b). While the temporal modulation is introduced by the modulation-frequency parameter,  $\Omega$ , the space modulation is introduced by our setting of the phase  $\varphi$  in Eq. (10) for each of the wires. To that end, we introduce the vector  $\vec{\zeta} = \hat{x}\zeta \cos \xi + \hat{y}\zeta \sin \xi$  in the  $x$ - $y$  plane, which represents the direction and magnitude at which the capacitor's phase  $\varphi$  is accumulated. Thus, to achieve the effect of synthetic motion, we choose the phase of the capacitance of the wire with indices  $(m, l)$  to be  $\varphi_{m,l} = \vec{\zeta} \cdot \vec{R}_{m,l} = m\zeta \cos \xi + l\zeta \sin \xi$ . By controlling the phase-modulation direction, we obtain spatial dispersion as shown below. Spatial dispersion by a spatiotemporally modulated metasurface was demonstrated in Refs. [49,50]. It is also an inherent property of infinite

stationary wire media when propagation occurs at least partially along the wires, and hence is also a fundamental property when finite wires or semi-infinite wires are used, because of the termination effect that excites wave spectra in various directions of propagation [31–37]. Substantial spatial dispersion may also be achieved by different means; for example, Boyd *et al.* [51] used dielectric rods with different diameters instead of a constant loaded wire. As opposed to these examples, in our case the spatial dispersion is obtained for propagation with wave vectors that are completely perpendicular to the wires, with infinite and physically uniform wires. It is obtained, and can be controlled, solely by the spatiotemporal modulation.

From Floquet-Bloch theorem, the current in the wire indexed  $m, l$  takes the form

$$I_{m,l} = \sum_{n=-\infty}^{\infty} A_n e^{-j\vec{q}_n \cdot \vec{R}_{m,l}} \delta(\omega - \omega_n), \quad (16)$$

where  $n$  represents the temporal harmonic number, and the corresponding wave vector is given by (see Appendix C for the derivation)

$$\vec{q}_n = \vec{q}_0 + n\vec{\zeta}, \quad (17)$$

with  $\vec{q}_0 = \hat{x}q_{0,x} + \hat{y}q_{0,y} = \hat{x}q_0 \cos \theta_0 + \hat{y}q_0 \sin \theta_0$ . Note that  $\vec{q}_0$  represents the corresponding wave vector at the nominal frequency  $\omega_0$ , and therefore  $\theta_0$  denotes the direction of propagation, with respect to the  $x$  axis, along the  $x$ - $y$  plane. We can now use the expression for the local field, and derive the dispersion relation and the equations for the eigenmodes. We follow the approach applied for a stationary medium in Sec. II, and perform the necessary modifications due to the spatiotemporal modulation of the medium. Assuming an infinite lattice, with currents given by Eq. (16), the local field on the  $(m, l) = (0, 0)$  wire reads

$$E^{\text{loc}} = \sum_{n=-\infty}^{\infty} E_n^{\text{loc}} \delta(\omega - \omega_n) = - \sum_{n=-\infty}^{\infty} \sum_{m,l \neq 0,0} A_n G_{nml} e^{-j\vec{q}_n \cdot \vec{R}_{m,l}} \delta(\omega - \omega_n), \quad (18)$$

where  $G_{nml} = (\eta k_n / 4) H_0^{(2)}(k_n R_{ml})$ , where  $R_{ml} = \sqrt{(ma)^2 + (lb)^2}$  and  $k_n = \omega_n / c$ , denoting the two-dimensional Green's function at the  $n$ th harmonic for a source located at  $\vec{R}_{ml}$  and observer at  $\vec{R}_{00}$ . By applying Eq. (18) with Eq. (12) and balancing between equal harmonics at the two sides of the resulting equation, we find a recursive relation between the different temporal harmonics of the induced current in the  $(m, l) = (0, 0)$

wire:

$$a_n A_{n-1} + b_n A_n + c_n A_{n+1} = 0, \quad (19)$$

where

$$a_n = \frac{m}{2} \frac{1}{\omega_{n-1} \tilde{C}_0}, \quad (20a)$$

$$b_n = \frac{\eta k_n}{2} \left[ \frac{1}{\pi} \ln \frac{b}{2\pi r_0} + \frac{1}{b\beta_{n,x}^{(l)}} \frac{\sin \beta_{n,x}^{(l)} a}{\cos \beta_{n,x}^{(l)} - \cos q_{n,x} a} + \sum_{l \neq 0} \left( \frac{1}{b\beta_{n,x}^{(l)}} \frac{\sin \beta_{n,x}^{(l)} a}{\cos \beta_{n,x}^{(l)} - \cos q_{n,x} a} - \frac{1}{2\pi |l|} \right) - \frac{1}{\omega_n \tilde{C}_0} \right], \quad (20b)$$

$$c_n = \frac{m}{2} \frac{1}{\omega_{n+1} \tilde{C}_0}, \quad (20c)$$

with  $\beta_{n,x}^{(l)} = -j \sqrt{[q_{n,y} + (2\pi l/b)]^2 - k_n^2}$ ,  $\text{Re}\{\sqrt{\cdot}\} > 0$ . For a dense grid, as in Sec. II, we approximate  $b_n$  in Eq. (20b):

$$b_n = \omega_n \tilde{L} - \frac{1}{\omega_n \tilde{C}_0} - \frac{\eta k_n}{ab(k_n^2 - q_n^2)}, \quad (21)$$

with

$$q_n^2 = (\vec{q}_0 + n\vec{\zeta})^2 = q_0^2 + 2n\zeta q_0 \cos \gamma + n^2 \zeta^2. \quad (22)$$

Here  $(\vec{x})^2 = \vec{x} \cdot \vec{x}$  and  $\gamma = \theta_0 - \xi$ . In Eq. (21),  $\tilde{C}_0 = C_0 \Delta$  as before and

$$\tilde{L} = \tilde{L}_w + \tilde{L}_0, \quad \text{with } \tilde{L}_0 = \frac{L_0}{\Delta}, \quad (23)$$

where  $L_0$  is an inductance that may be connected in series with the loading capacitor  $C(t)$ . Effectively it simply increases the intrinsic wire inductance. As in the case of stationary wire medium with a dense grid, also here the approximation for  $b_n$  in Eq. (21) depends only on  $q_n^2$ , whereas the exact expression for  $b_n$  in Eq. (20b) also depends on  $q_{n,x}$ .

As opposed to the stationary-loaded-wire-medium case, where the effective longitudinal permittivity may be analytically expressed using Eq. (8) with Eq. (9), for the spatiotemporally modulated case, the interaction between the different temporal-frequency harmonics should be included. To that end, Eq. (19) is used. The latter can be represented using a tridiagonal matrix of infinite rank. We assume that for large-enough  $N$ , the currents

$A_{-(N+1)}, A_{N+1}$  are negligible. In this case the infinite matrix can be approximated by a finite square matrix:

$$\underline{\underline{A}}^N = \begin{pmatrix} \ddots & \ddots & 0 & 0 & & & & \\ \ddots & b_{-2} & c_{-2} & 0 & 0 & & & \\ 0 & a_{-1} & b_{-1} & c_{-1} & 0 & 0 & & \\ 0 & 0 & a_0 & b_0 & c_0 & 0 & 0 & \\ & 0 & 0 & a_1 & b_1 & c_1 & 0 & \\ & & 0 & 0 & a_2 & b_2 & \ddots & \\ & & & 0 & 0 & \ddots & \ddots & \end{pmatrix}. \quad (24)$$

For nontrivial wave solutions, we look for the dispersion relation  $\vec{q}_0(\omega)$  that nullifies the determinant,

$$|\underline{\underline{A}}^N| = 0. \quad (25)$$

In the following we explore the wave dynamics in the bulk as obtained from this dispersion relation for a particularly interesting case near the plasma frequency of the corresponding stationary wire medium. [?pag ?>](#)

#### IV. NEAR THE PLASMA FREQUENCY OF THE STATIONARY MEDIUM

In the following we explore the wave dynamics of the spatiotemporally modulated medium with parameters that are near the plasma frequency of the corresponding stationary medium; namely, with  $\omega = \omega^0 + \delta\omega$ , where  $\omega^0$  is the frequency that nullifies  $\varepsilon_z(\omega)$  in Eq. (8). Thus, [?pag ?>](#)

$$\omega^0 = \sqrt{\frac{1}{\tilde{L}} \left( \frac{1}{\tilde{C}_0} + \frac{1}{\tilde{C}_b} \right)} = \sqrt{\frac{1}{\tilde{L}\tilde{C}_0}} \sqrt{1 + \psi}, \quad (26)$$

where  $C_b$  is defined after Eq. (9), and [?pag ?>](#)

$$\psi = \frac{\tilde{C}_b}{\tilde{C}_0}. \quad (27)$$

In the following we also use  $k^0 = \omega^0/c$ . [?pag ?>](#)

##### A. Analytical approximation for the lower-order solutions with weak modulation

We assume weak modulation,  $m \ll 1$ , and as a result the dominant harmonics besides the fundamental one will be  $n = \pm 1$ . This assumption excludes the possibility that higher-order harmonics will be strongly excited in this case due to the presence of some resonance mechanism at some other frequency. Under this assumption, the infinite-rank matrix  $\underline{\underline{A}}$  is replaced by a tridiagonal  $3 \times 3$  matrix  $\underline{\underline{A}}^1$  [ $N = 1$  in Eq. (25)]. The dispersion relation in this case is found by nullifying its determinant, i.e.,

$$\frac{a_0 c_{-1}}{b_{-1}} + \frac{a_1 c_0}{b_1} = b_0. \quad (28)$$

By plugging in the expressions for  $a_n$  and  $c_n$  that are given in Eq. (20a), with the dense-grid approximation Eq. (21),

together with Eq. (27), and with  $q_1$  and  $q_{-1}$  given in Eq. (17), the nontrivial-solution requirement in Eq. (28) turns into a sixth-order polynomial equation for  $q_0$ :

$$\frac{m^2 \psi^2}{4} \left( \frac{1}{X_{-1}(\omega, q_0)} + \frac{1}{X_1(\omega, q_0)} \right) = X_0(\omega, q_0), \quad (29a)$$

with

$$X_n(\omega, q_0) = \frac{k_n^2}{(k^0)^2} (1 + \psi) - \psi - \frac{k_n^2}{k_n^2 - q_n^2}. \quad (29b)$$

We denote the  $n$ th root of Eq. (29a) by  $q_0^{(n)}$ , where  $n = 1, \dots, 6$ . Two of the six solutions of this polynomial equation will represent a *perturbation over the two solutions of the corresponding stationary wire medium*. Since we focus here on the dispersion near the plasma frequency of the corresponding stationary medium (i.e., in the vicinity of  $\omega^0$ ), it is reasonable to assume that two of the solutions satisfy  $q_0^{(1)}, q_0^{(2)} \ll k^0$ . In that case, on the left-hand-side of Eq. (29a) we use  $\omega = \omega^0$  and  $q_0 = 0$ , and thus  $X_1, X_{-1} \sim 1$ . Since  $m \ll 1$ , the plasma frequency of the spatiotemporally modulated medium (namely, the fre-

quency at which  $q_0^{(1)}$  and  $q_0^{(2)}$  experience the transition from being purely imaginary to purely real) shifts by  $\delta\hat{\omega}$  with respect to  $\omega^0$  of the stationary medium, where

$$\frac{\delta\hat{\omega}}{\omega^0} \approx \left( \frac{1}{X_1(\omega^0, 0)} + \frac{1}{X_{-1}(\omega^0, 0)} \right) \frac{m^2 \psi^2}{8(1 + \psi)}. \quad (30)$$

The first two solutions,  $q_0^{(1)}$  and  $q_0^{(2)}$ , for the fundamental modes up to the shift in  $\delta\hat{\omega}$  are obtained by solving  $X_0(\omega, q_0) = 0$  and are given by

$$q_0^{(1,2)} = \pm k^0 \left( 1 + \frac{\delta\omega}{\omega^0} - \frac{\delta\hat{\omega}}{\omega^0} \right) \times \sqrt{1 - \frac{1}{[1 + (\delta\omega/\omega^0) - (\delta\hat{\omega}/\omega^0)]^2 (1 + \psi) - \psi}}. \quad (31)$$

We can see that under the dense-grid approximation, solutions No. 1 and No. 2 are isotropic, independent of the relative angle  $\gamma$  between the spatiotemporal-modulation axis and the direction of wave propagation.

To find the other four roots of Eq. (29a) we assume that these solutions are not small compared with  $k^0$  near  $\omega^0$ . As a result, the right-hand side of Eq. (29a)  $X_0(\omega^0, q_0) \sim 1$ . On the other hand, in light of the small factor  $m^2$  on the left-hand side, the only way to balance the two sides is if either  $X_1$  or  $X_{-1}$  is nearly vanishing. Therefore, the remaining four roots are approximated by solving  $X_1(\omega, q_0) = 0$  and  $X_{-1}(\omega, q_0) = 0$ . Each of the equations yields two solutions:

$$q_0^{(3,4)} = -\zeta \cos \gamma \pm k_1 \sqrt{-\left(\frac{\zeta}{k_1}\right)^2 \sin^2 \gamma + 1 - \frac{1}{[k_1^2/(k^0)^2](1 + \psi) - \psi}}, \quad (32a)$$

$$q_0^{(5,6)} = \zeta \cos \gamma \pm k_{-1} \sqrt{-\left(\frac{\zeta}{k_{-1}}\right)^2 \sin^2 \gamma + 1 - \frac{1}{[k_{-1}^2/(k^0)^2](1 + \psi) - \psi}}. \quad (32b)$$

If imaginary, the square roots in Eqs. (31) and (32) should be chosen to guarantee physical solutions; namely, the wave must decay at infinity. In Fig. 3 we show the dispersion of the six solutions as obtained by the analytical approximated relations in Eqs. (31) and (32); the dispersion is shown for the following structure parameters:  $a = 0.07\lambda^0$ ,  $b = 0.1\lambda^0$ ,  $r_0 = 0.0001\lambda^0$ , and  $\theta_0 = 0$ . As opposed to the structural parameters, the *modulation* parameters differ between four typical cases as summarized in Table I. The complex dispersion diagrams, real and imaginary  $q_0$ , are shown as a function of  $\delta\omega$ , which is the detuning frequency from  $\omega^0$ —the plasma frequency of the stationary lattice. In all four cases the lines are color-coded, blue for  $q_0^{(1,2)}$ —the perturbation on the solution of the stationary medium—and green and red for the new solutions due

to the spatiotemporal modulation,  $q_0^{(3,4)}$  and  $q_0^{(5,6)}$ , respectively. The colored lines in Fig. 3 are obtained by our using the approximated solutions that are given in Eqs. (31), (32a), and (32b) to show the analytical approximation validity. As a comparison in the plots we also draw by black circles the numerical solution of Eq. (29a).

The good agreement between the analytical approximations and the numerical calculations allow us to use our analytical results for synthesis. For example, an interesting characteristic for the roots of  $q_0^{(3)}$ ,  $q_0^{(4)}$ ,  $q_0^{(5)}$ , and  $q_0^{(6)}$  is that we can create a different response for different angles  $\gamma$  and in particular reach effective Fresnel drag dispersion accompanied with strong anisotropy for waves propagating in the wire-medium bulk by using *slow* spatiotemporal modulation.

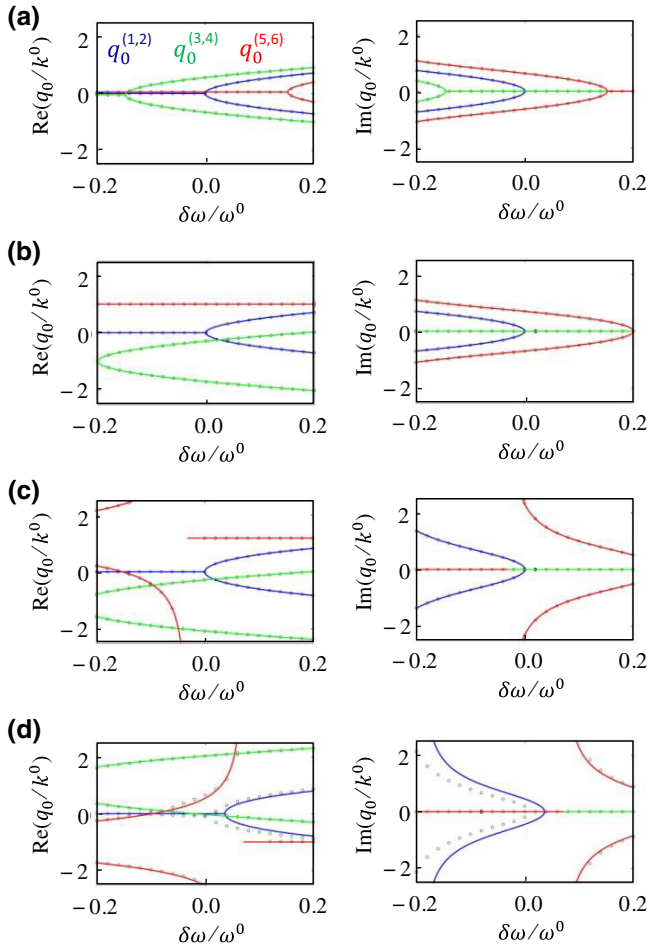


FIG. 3. Dispersion relations as obtained by solutions No. 1–No. 6 in Eqs. (31) and (32). The fundamental wave number  $q_0$  of each of the solutions is shown as a function of the frequency  $\delta\omega/\omega_0$  for the four parameter cases that are tabulated in Table I: (a) case I, (b) case II, (c) case III, and (d) case IV. Continuous lines represent the analytical results and circles represent the numerical results.

TABLE I. Four parameter cases used in the numerical calculations in Sec. IV.

	$m = \delta C/C_0$	$\Omega/\omega^0$	$\zeta/k^0$	$\tilde{L}_0/\tilde{L}_w$	$\xi$	$\psi$
Case I	0.1	0.15	0.1	4.3	$-\pi/3$	0.27
Case II	0.35	0.2	1.0	4.0	0	0.2
Case III	0.06	0.25	1.2	7.6	$\pi/20$	1.07
Case IV	0.25	0.3	1.0	9.3	$-\pi$	1.47

## B. Effective Fresnel drag with weak and slow spatiotemporal modulation

The spatiotemporal modulation enables us to achieve dispersion that shares similarities with the dispersion of waves in a moving medium. However, typically this effect at the fundamental harmonic frequency is rather weak and requires time modulation much faster than the guided signal frequency [40]. This is not the case, however, when we spatiotemporally modulate the loaded wire medium. In this section we show that it is the *interplay* between the *spatiotemporal modulation* and the *cutoff of the stationary mode*,  $q_0^{(1,2)}$ , below  $\omega^0$ —the plasma frequency of the corresponding stationary medium—that enables us to obtain effective Fresnel drag with no actual motion and using slow and weak modulation at the fundamental frequency of one of the higher-order modes (e.g.,  $q_0^{(3,4)}$ ). To see this effect, we use Eqs. (31), (32a), and (32b) to extract the relation between  $\delta\omega$  and the transverse wave-number components  $q_{0x} = q_0 \cos \theta_0$  and  $q_{0y} = q_0 \sin \theta_0$  for a given set of medium and modulation parameters. By solving Eq. (31) for  $\delta\omega$ , we obtain

$$\frac{\delta\omega^{(1,2)}}{\omega^0} = \frac{\delta\hat{\omega}}{\omega^0} + \frac{q_0^2/2(k^0)^2}{\left(1 + \psi \left[1 - [q_0^2/(k^0)^2]\right]\right)}, \quad (33)$$

whereas by solving Eqs. (32a) and (32b) for  $\delta\omega$ , we get

$$\frac{\delta\omega^{\pm 1}}{\omega^0} = \frac{1 + \{1 - [\psi/(1 + \psi)]\} [q_{\pm 1}^2/(k^0)^2] - [1 \pm (\Omega/\omega^0)]^2}{4[1 \pm (\Omega/\omega^0)]^2 - 2 \left\{1 + [q_{\pm 1}^2/(k^0)^2]\right\}}, \quad (34)$$

where  $+1$  ( $-1$ ) corresponds to solutions No. 3 and No. 4 (No. 5 and No. 6) in Eq. (32), and  $q_{\pm 1}$  is given by Eq. (22). In the latter we note that  $q_0^2 = q_x^2 + q_y^2$ ,  $\gamma = \theta_0 - \xi$ , where  $\xi$  is the direction of the modulation and  $\tan \theta_0 = q_y/q_x$ . These dispersion relations are shown in Fig. 4 for the parameters of case III in Table I. In Fig. 4(a) with  $\xi = 0$ , a color map that shows  $\delta\omega/\omega_0$  as a function of the transverse wave vector  $(q_x, q_y)$  is presented, showing that the

fundamental solutions are propagating only at positive frequencies [to be more precise,  $(\delta\omega/\omega^0)^{(1,2)} = (\delta\hat{\omega}/\omega^0) \approx 0$ ]. However, the  $\pm 1$  solutions [see Eq. (34)], with strongly *asymmetric* dispersion, are propagating at *negative* frequencies, as shown in Figs. 4(b) and 4(c). As a result, in the spatiotemporally modulated wire medium, effective motion may be exhibited at the *fundamental propagating harmonic* and with slow modulation. This behavior may

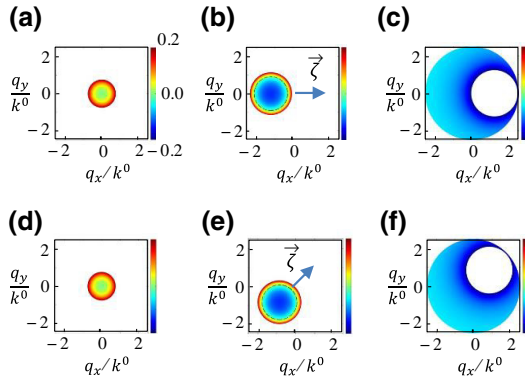


FIG. 4. Dispersion diagrams for the fundamental solutions No. 1 and No. 2 and higher-order solutions No. 3–No. 6 for the parameters for case III in Table I. (a) With  $\xi = 0$  the dispersion for the fundamental solutions  $q_0^{(1,2)}$  is centered at the origin of the  $q_x$ - $q_y$  plane; however, its cutoff frequency is  $\delta\omega/\omega_0 \approx 0$ . (b) In contrast, the higher-order solutions  $q_0^{(3,4)}$  are propagating already at negative frequencies. These solutions are essentially nonreciprocal in light of their asymmetric dispersion. (c) is as (b) but for the additional solutions  $q_0^{(5,6)}$ . (d)–(f) are as (a)–(c) but with  $\xi = \pi/4$ .

be controlled by adjustments of the direction of modulation, as shown in Fig. 4(d) for the fundamental solution, and in Figs. 4(e) and 4(f) for the  $\pm 1$  harmonic, this time with spatiotemporal modulation along the tilted,  $\xi = \pi/4$  direction.

## V. HOMOGENIZATION

### A. Effective modal permittivity

Using the wave-number dispersion of the modal solutions given in Eqs. (31) and (32), one can define effective permittivity for each of the modal solutions found above. To that end we first write the free-space wave number as

$$k^2 = (k^0)^2 \left( 1 + \frac{\delta\omega}{\omega^0} \right)^2. \quad (35)$$

Then the homogenized effective permittivity of the modal solution No.  $i$  is given by

$$\varepsilon_{r,i} = \left( q_0^{(i)} \right)^2 / k^2. \quad (36)$$

This effective relative permittivity connects the free-space wave number with the guided-mode wave number, at the *fundamental* harmonic, of each of the modal solutions. It is important to stress that each of these modes, with  $q_0^{(i)}$ , consists of infinite space-time harmonics as dictated by Eq. (16). Once  $\varepsilon_{r,i}$  is known,  $q_0^{(i)}$  can be calculated. Then, using Eq. (17), the wave number of each of the infinite harmonics that forms the  $i$  modal solution is immediately found. Specifically, for the first six fundamental modal solutions in the spatiotemporally modulated wire medium we have

$$\varepsilon_{r,1} = \varepsilon_{r,2} = \left( \frac{1 + (\delta\omega/\omega^0) - (\delta\hat{\omega}/\omega^0)}{1 + (\delta\omega/\omega^0)} \right)^2 \left( 1 - \frac{1}{[1 + (\delta\omega/\omega^0) - (\delta\hat{\omega}/\omega^0)]^2 (1 + \psi) - \psi} \right), \quad (37a)$$

$$\varepsilon_{r,3,4} = \frac{1}{[1 + (\delta\omega/\omega^0)]^2} \left[ -\frac{\zeta}{k^0} \cos \gamma \pm \frac{k_1}{k^0} \sqrt{-\left( \frac{\zeta}{k_1} \right)^2 \sin^2 \gamma + 1 - \frac{1}{[k_1^2/(k^0)^2] (1 + \psi) - \psi}} \right]^2, \quad (37b)$$

$$\varepsilon_{r,5,6} = \frac{1}{[1 + (\delta\omega/\omega^0)]^2} \left[ \frac{\zeta}{k^0} \cos \gamma \pm \frac{k_{-1}}{k^0} \sqrt{-\left( \frac{\zeta}{k_{-1}} \right)^2 \sin^2 \gamma + 1 - \frac{1}{[k_{-1}^2/(k^0)^2] (1 + \psi) - \psi}} \right]^2. \quad (37c)$$

As evident from Eq. (37a), clearly the effective permittivities that correspond to the first two modal solutions exhibit a reciprocal behavior and are independent of the direction of propagation, and moreover they become positive only above  $\delta\omega/\omega_0 \approx 0$ . This is what we expect from the *stationary* wire medium as given in Eq. (8). This is reasonable since these two solutions in the spatiotemporally modulated wire medium are essentially a weak *perturbation* over the solutions of the conventional stationary

wire medium. Note, however, that from comparison of the terms in Eq. (8) and (37a), it is clear that the modulation parameters affect to some extent the values of the permittivity, albeit not its general properties. Moreover, while Eq. (37a) exhibits a reciprocal, stationary-medium-like, behavior, there are additional higher-order harmonics [see Eq. (17)] that break the reciprocity. As opposed to  $\varepsilon_{r,1,2}$ , the additional effective permittivities (i.e.,  $\varepsilon_{r,3}$  etc.) demonstrate a substantial nonreciprocity already at the



fundamental harmonic. Even more important is the fact that these solutions are propagating already with negative frequencies  $\delta\omega/\omega_0 < 0$  in the region where the first two solutions are evanescent. This implies, as we discussed in the previous section in the context of Fresnel drag, that a substantial nonreciprocity can be observed in the spatiotemporally modulated wire medium already with weak-modulation and slow-modulation parameters. We also stress that these modes are propagating below the plasma frequency for any modulation depth  $m$ , even if extremely small. Therefore, these modes share similarities with the extraordinary whistler mode in magnetoplasma that also propagates below the plasma frequency with any magnetic biasing [39]. This behavior is shown in Fig. 5, which shows for the parameters that are given in case II in Table I a plot of the effective permittivity for the first six fundamental modal solutions as a function of  $\delta\omega/\omega^0$  and for two main situations: in Figs. 5(a) and 5(b), real and imaginary parts, where the propagation is parallel to the modulation axis,  $\vec{q}_0 \parallel \vec{\zeta}$ , and in Figs. 5(c) and 5(d) where  $\vec{q}_0 \perp \vec{\zeta}$ . The effective permittivity for the stationary (LTI) medium is shown as black circles, while the solutions

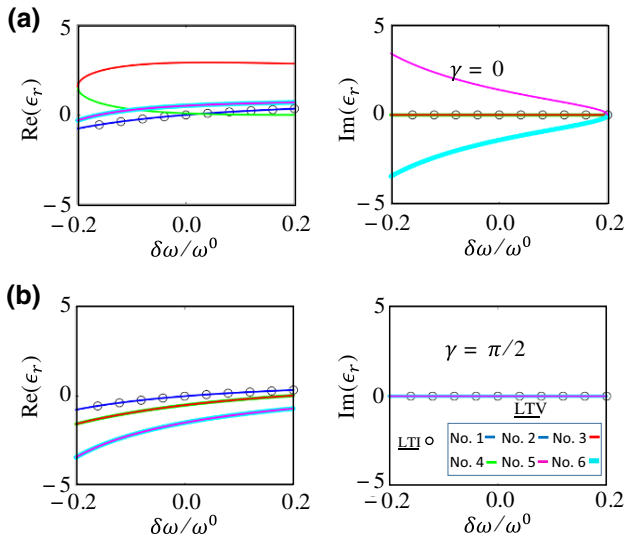


FIG. 5. Effective permittivity of a spatiotemporally modulated wire medium. Parameters for case II in Table I. (a) Effective permittivity of the modal solutions when the propagation is collinear with the modulation. Circles represent no modulation (stationary wire media). Fundamental modal solutions No. 1,2 (continuous blue lines) are nearly identical to these of the stationary-medium solutions and are reciprocal. The higher-order solutions No. 3,4 and No. 5,6 exhibit deviation with respect to the stationary-medium solutions and substantial nonreciprocity. (b) is as (a) but for propagation normal to the direction of modulation. The solutions are reciprocal in this case, and thus the strong anisotropy due to the spatiotemporal modulation clearly emerges from comparison of (a),(b). LTV, linear time variant.

for the spatiotemporally modulated lattice are shown as colored lines.

In Fig. 5 high anisotropy is evident due to the directional preference dictated by the spatiotemporal-modulation vector  $\vec{\zeta}$ . In addition, the two fundamental solutions No. 1 and No. 2 are essentially identical to the two counterpropagating solutions of the corresponding stationary (LTI) medium (shown in black circles), and as such they propagate only with  $\delta\omega > 0$ . In contrast, the higher order solutions may be highly nonreciprocal, except for the case where the propagation is transverse to the modulation vector [Figs. 5(c) and 5(d)]. As an example, see the counterpropagating solutions No. 3 and No. 4 in Fig. 5(a) that are associated with different effective permittivities. Moreover, it is seen that the spatiotemporal modulation yields a magnetized plasmlike extraordinary wave propagation in the sense that propagation becomes allowed with any modulation index below the so-called plasma-frequency  $\omega^0$ . As opposed to Fig. 5, which uses  $\psi = 0.2 \ll 1$ , in Fig. 6 we show similar results but with larger capacitive loading, so  $\psi = 1.07 \sim 1$ . Here the effect of the spatiotemporal modulation becomes stronger, as evident from a comparison between Figs. 5 and 6. Also here, the fundamental solutions No. 1 and No. 2 exhibit permittivity that is essentially identical to that of the corresponding unmodulated lattice. However, as opposed to Fig. 5, here the extraordinary modes that are supported below the plasma frequency are much-more dispersive, and the nonreciprocity becomes more dominant, as can be seen by comparing the counterpropagating solution pairs No. 3,4 and No. 5,6. We demonstrate and discuss in Sec. VII that as opposed to the effective permittivities that are shown in Fig. 6 for the

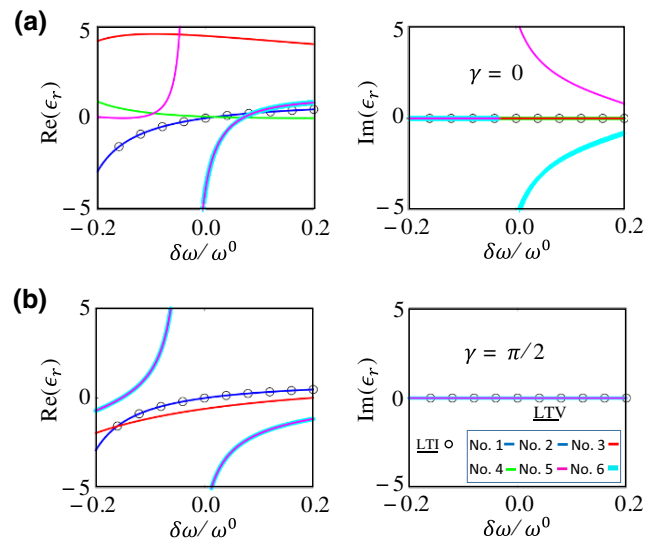


FIG. 6. Effective permittivity of the modal solutions for case III in Table I. As in Fig. 5 except that that  $\psi \sim 1$  implies a much-stronger effect by the modulation as evident from comparison with Fig. 5. LTV, linear time variant.

parameters in case III, the effective permittivities shown in Fig. 5 for the parameters in case II can be adequately reproduced in a model in which the spatiotemporal modulation is introduced after the homogenization.

### B. Averaged field equations and Poynting vector

For each of the modal solutions, with  $q_0 = q_0^{(i)}$ , we write the governing electrodynamic equations for the *averaged* fields. We begin by calculating the average fields in the unit cell at the origin. To that end, we use the expression for the currents in Eq. (2). For the fundamental harmonic of each of the modal solutions, the electric field can be written in the same way as in Eq. (4), but with the modification for the entire unit cell, except on the wire itself:

$$\begin{aligned}\vec{E}(\vec{r}) &= -\frac{\hat{z}\eta k}{4} \sum_{m,l} H_0^{(2)}(k|\vec{R}_{ml} - \vec{r}|) I_0 e^{-j(q_x a m + q_y b l)} \\ &= -\frac{\hat{z}\eta k I_0}{2} \sum_{m=-\infty}^{\infty} S_m(\vec{r}) e^{-j q_x a m},\end{aligned}\quad (38)$$

with

$$\begin{aligned}S_m(\vec{r}) &= \frac{1}{2} \sum_{l=-\infty}^{\infty} H_0^{(2)}(k|\vec{R}_{ml} - \vec{r}|) e^{-j q_y b l} \\ &= -\frac{1}{b} \sum_{l=-\infty}^{\infty} \frac{e^{j y [q_y + (2\pi l/b)]} e^{-j a |m - (x/a)| \beta_{x,l}}}{\beta_{x,l}}.\end{aligned}\quad (39)$$

The last summation in Eq. (39) is obtained with the aid of Poisson summation. This summation is rapidly converging and can be expressed in closed form using a geometric series. This finally leads to an expression for the electric field, with separation between the first propagating harmonic and the remaining Floquet harmonics, which are all evanescent in the dense-grid approximation, and as long as the modulation frequency is low enough so that the array can be considered as dense also at the highest temporal harmonic  $\omega_n$ , which cannot be ignored (see Appendix D):

$$\vec{E}(\vec{r}) \approx -\frac{\hat{z}\eta k I_0}{2b} \left[ \begin{aligned} &\frac{(1+jyq_y)}{\sqrt{k^2-q_y^2}} \left( 1 + \frac{1-j(a+x)\sqrt{k^2-q_y^2}+jq_x a}{ja\sqrt{k^2-q_y^2}-jq_x a} + \frac{1-j(a-x)\sqrt{k^2-q_y^2}-jq_x a}{ja\sqrt{k^2-q_y^2}+jq_x a} \right) \\ &-2 \sum_{l=1}^{\infty} \frac{e^{jy(2\pi l/b)}(1+jq_y y)}{(2\pi l/b+q_y)} \left( \begin{aligned} &e^{-|x|(2\pi l/b)}(1-q_y|x|) + \frac{e^{-2\pi l[(a+x)/b]}(1-q_y a+jq_x a-q_y x)}{1-e^{-2\pi l(a/b)}(1-q_y a+jq_x a)} \\ &+ \frac{e^{-2\pi l[(a-x)/b]}(1-q_y a+jq_x a+q_y x)}{1-e^{-2\pi l(a/b)}(1-q_y a-jq_x a)} \end{aligned} \right) \end{aligned} \right]. \quad (40)$$

To simplify the calculation of the average fields inside the unit cell, since the wire is assumed to be thin  $r_0 \ll a, b$  we ignore the fact that the field inside the perfect-electric-conductor wire is zero. This simplification enables us to perform integration inside the unit cell without complicated boundaries. This assumption is supported by the fact that

$$\frac{2\pi \int_0^{r_0} E^w r dr}{ab} = 2\pi \frac{\eta k I_0}{4ab} \int_0^{r_0} H_0^{(2)}(kr) r dr \sim O\left(\frac{r_0^2}{ab} \ln kr_0\right), \quad (41)$$

which implies that the resulting error by this approximation is  $O(r_0^2/ab)$ . The average field is then calculated by

$$\langle \vec{E} \rangle \approx \frac{1}{ab} \int_{-(a/2)}^{(a/2)} \int_{-(b/2)}^{(b/2)} \vec{E}(\vec{r}) dx dy. \quad (42)$$

Thus,

$$\langle \vec{E} \rangle \approx -\frac{\hat{z}\eta k I_0}{2} \left( \begin{aligned} &\frac{2}{jab(k^2-q_0^2)} - \frac{1}{b\sqrt{k^2-q_y^2}} \\ &-2 \sum_{l=1}^{\infty} \frac{q_y b(-1)^l}{2l\pi a[(2\pi l/b)+q_y]} \left( \begin{aligned} &\frac{-q_y b+2l\pi+e^{-l\pi(a/b)}(q_y a l\pi+q_y b-2l\pi)}{2l^2\pi^2} \\ &+ \left( \frac{2e^{-(2\pi l(a/b)+q_y a-jq_x a)} \sinh(a/2)[(2\pi l/b)+q_y]}{b[(2\pi l/b)+q_y]} \right) \right) \\ &\times \left( \frac{1}{1-e^{-2\pi l(a/b)}(1-q_y a+jq_x a)} \right) \\ &+ \left( \frac{1}{1-e^{-2\pi l(a/b)}(1-q_y a-jq_x a)} \right) \end{aligned} \right) \end{aligned} \right). \quad (43)$$

For a dense array, the infinite summation in Eq. (43) can be ignored, and thus the average field may be simplified as

$$\langle \vec{E} \rangle \approx -\hat{z}\eta k I_0 \left( \frac{1}{jab(k^2 - q_0^2)} - \frac{1}{2b\sqrt{k^2 - q_y^2}} \right). \quad (44)$$

The result in Eq. (44) is in good agreement with Ref. [22] (see Appendix E). Following Ref. [30], we can write the relation between the macroscopic (averaged) fields:

$$\vec{\nabla} \times \vec{E}_{\text{macro}} = -j\omega\mu_0 \vec{H}_{\text{macro}}, \quad (45a)$$

$$\vec{\nabla} \times \vec{H}_{\text{macro}} = \frac{I}{ab} \hat{z} + j\omega\varepsilon_0 \vec{E}_{\text{macro}}. \quad (45b)$$

Therefore, the macroscopic magnetic field

$$\vec{H}_{\text{macro}} = -\frac{1}{jk\eta} \vec{\nabla} \times \vec{E}_{\text{macro}} = -\frac{1}{jk\eta} j\vec{q}_0 \times \langle \vec{E} \rangle. \quad (46)$$

The average Poynting vector reads [30]

$$S_{\text{avg}} = \frac{1}{2} \text{Re} \left( \vec{E}_{\text{macro}} \times \vec{H}_{\text{macro}}^* + \frac{\varphi_w I^*}{ab} \hat{z} \right). \quad (47)$$

Since in our case the currents are independent of  $z$ ,  $\varphi_w = 0$ , and we may write

$$S_{\text{avg}} = \frac{1}{2} \text{Re} (\vec{E}_{\text{macro}} \times \vec{H}_{\text{macro}}^*) = \frac{q_0}{2k\eta} |\langle E \rangle|^2. \quad (48)$$

## VI. EXCITATION OF A FINITE SAMPLE

In the previous sections we explored analytically the modal solutions that are supported in an infinite spatiotemporally modulated wire medium. These solutions expand, partly, the spectra of waves that are expected to be observed on the excitation of a finite lattice. In this section we study numerically the excitation problem of a finite lattice of infinite wires. These simulations model the practical problem of a wire medium that is located between the plates of a parallel-plate waveguide with electrically small spacing between the plates so that only a TEM mode may be supported. Specifically, we aim to verify the analytical derivations of the infinite lattice that were performed in the previous sections, and moreover, we strive to bring additional physical insights concerning the wave dynamics in the presence of a plane wave or localized source. We emphasize that the numerical results in this section are limited in two aspects. First, they are fully numerical, while a complete semianalytical formalism of the full Green's function is still absent, but is currently undergoing exploration by our group. Second, our numerical simulations are concerned with a finite lattice of infinite wires, which models effectively the practical problem of

spatiotemporally modulated wires inside a parallel-plate waveguide. We emphasize, however, that our current simulation approach is inadequate to analyze the propagation inside a spatiotemporally modulated lattice of *finite* (or semi-infinite) wires. Studying the finite-wire problem is of practical significance and this problem will exhibit substantial nonlocality by the termination of the wires, and not only by the spatiotemporal modulation [31–37]. However, it requires an ad hoc numerical approach that is capable of taking into account the time variation, and simultaneously be reasonable in terms of the computational resources that are needed to consider an electrically large sample that consists of deep-subwavelength elements. We stress that due to the spatiotemporal modulation, using the structural periodicity is, in general, impossible unless specific conditions for the spatial-modulation periodicity and the structural periodicity are met. These, of course, are not satisfied in general, and thus Floquet boundary conditions, which are commonly used to computationally relax the analysis of periodic structure calculations, cannot be used for our system.

In Fig. 7 we explore the scattering of an impinging plane wave at a finite lattice of infinite wires. In Fig. 7(a) the simulated structure is illustrated. A  $z$ -polarized plane wave propagates toward the positive  $x$  axis and impinges on a finite lattice of spatiotemporally modulated wires. The array consists of  $N_x \times N_y$  wires, where  $N_x = 201$  and  $N_y = 141$ , where the unit-cell parameters are  $a = 0.07\lambda^0$  and  $b = 0.1\lambda^0$ , so the entire sample shape is nearly a square. With these parameters, the array size is about  $14\lambda^0 \times 14\lambda^0$ , where  $\lambda^0 = 2\pi c/\omega^0$ , where  $\omega^0$  denotes the “plasma frequency” of the corresponding stationary lattice as defined above. The remaining parameters are as given in cases III and IV in Table I, and are used in the simulations for the dispersion diagrams of the infinite lattice. For each wire in the finite lattice we write a self-consistent equation that relates the local field at the wire location, in the absence of the wire itself, to the induced current in the wire. The local field is connected to the current with use of the effective susceptibility expression that we develop for time-modulated wires in Appendix B. The loop is closed by our calculating the local field using the summation of the external exiting field plus the contribution at each frequency harmonic calculated by a two-dimensional Green's function in free space, evaluated at the proper frequency. This procedure yields a square linear system of rank  $(N_x \times N_y \times N)$ , where  $2N + 1 = 3$  is the number of temporal harmonics that we consider. Because of its size, solving this system is computationally expensive and is achieved with use of a Dell Precision workstation with 512 GB RAM. In Fig. 7(b), simulation results for case III at  $\delta\omega = -0.15\omega^0$  are shown. At this frequency the stationary lattice will not support any guided bulk wave. Only surface-plasmon-like waves are expected to be excited at the interface between the wire-medium bulk and the

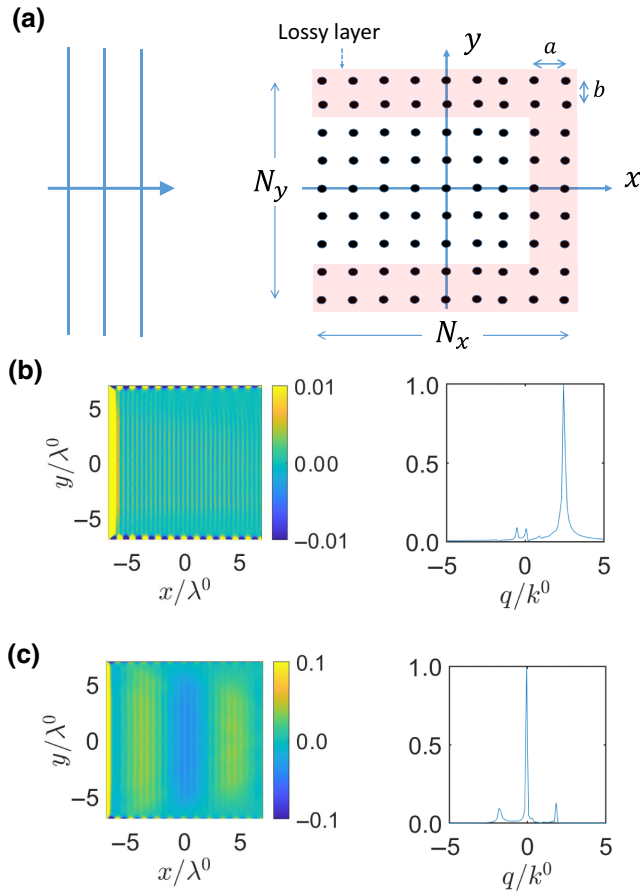


FIG. 7. (a) Illustration of the structure. A  $z$ -polarized plane wave propagates along the  $x$  axis and impinges on a finite lattice of spatiotemporally modulated wires. The array size is  $N_x = 201$ ,  $N_y = 141$  wires, with unit-cell parameters  $a = 0.07\lambda^0$  and  $b = 0.1\lambda^0$ , so the overall sample shape is nearly a square. The remaining parameters are as given in cases III and IV in Table I, and are used in the simulations for the dispersion diagrams of the infinite lattice. (b) For case III, at  $\delta\omega = -0.15\omega^0$ . The left panel shows a color map of the real part of the excited current wave, normalized by its maximal value. The strongly excited fundamental (stationary) solution is decaying rapidly, and the higher-order solutions are propagating. The right panel shows the discrete Fourier transform (implemented by FFT) carried over the field along  $y = 0$  reveals the excited spatial-frequency content, which nicely agrees with the dispersion calculations for the wave numbers of the wave that propagates along  $x$ . (c) As in (b) but for case IV in Table I.

surrounding vacuum. The left panel in Fig. 7(b) shown a color map of the real part of the excited current wave is shown. The current distribution is normalized by the maximal current amplitude detected on the sample. This panel shows the strong excitation of the evanescent dominant solution (stationarylike with  $q_0^{(1,2)}$ ), which rapidly decays to zero, whereas the higher-order solutions, due to the spatiotemporal modulation, are clearly propagating. At the top and bottom of the panel, surface-plasmon-like propagation occurs at the interface between the wire media

and the vacuum. These trapped modes are excited due to the sharp corners of the finite sample. To validate the analytical derivations that were performed for the infinite lattice in previous sections, in the right panel in Fig. 7(b), we show the discrete Fourier transform (implemented by MATLAB FFT) that is carried over the field along  $y = 0$ . This panel reveals the excited spatial frequency content, with dominant peaks at  $q/k^0 = -0.53$  and  $2.42$  and minor peaks at  $q/k^0 = -1.83$  and  $-0.02$ . This is in agreement with the dispersion-based calculations that predict the following modal wave numbers under the same conditions for the infinite lattice. Specifically, at  $\delta\omega = -0.15\omega^0$  the expected wave numbers for propagation along the  $x$  axis are  $q_0^{(1,2)}/k^0 = \pm 0.99j$  (evanescent fundamental solutions),  $q_0^{(3)}/k^0 = -0.61$ ,  $q_0^{(5)}/k^0 = 2.39$  (propagating toward the positive  $x$  axis), and  $q_0^{(4)}/k^0 = -1.76$ ,  $q_0^{(4)}/k^0 = -0.02$  (propagating toward the negative  $x$  axis). The latter are excited only due to the reflection at the right side of the sample. The existing deviations between the FFT calculation and the theoretical predictions are caused by a too-short sampling interval that limits the spectral resolution. To minimize the effect of multiple reflections inside the finite sample, we introduce lossy layers of wires at its perimeter. Specifically, we use  $N_{\text{loss},y} = 30$  lossy layers at the top and bottom sides of the sample and  $N_{\text{loss},x} = 40$  lossy layers at the right side of the sample. The lossy layers are implemented by the introduction of a serial resistor loading on each of the wires, in addition to the time-modulated capacitance and the tuning fixed inductance. On each layer the resistance is tapered with a square profile that goes from 0 to  $5\eta$  along the  $N_{\text{loss},x/y}$  layers of absorber. For example,  $R_{\text{loss}} = 5\eta[1 - (n - N_{\text{loss},x/y})^2/N_{\text{loss},x/y}^2]$ , where  $n = 1, \dots, N_{\text{loss},x/y}$ , where  $n = 1$  is the index of the innermost lossy layer and  $n = N_{\text{loss},x/y}$  denotes the outermost lossy layer. Thus, the absorber overall thickness is about  $2\lambda^0$  at each side. Fig. 7(c) is as Fig. 7(b) but for case IV. The right panel shows dominant peaks by FFT at  $q/k^0 = 1.83$  and  $-0.06$  and minor peaks at  $q/k^0 = 0.29$  and  $-1.83$ , compared with  $q_0^{(1,2)} = \pm 1.84j$  (evanescent),  $q_0^{(3)}/k^0 = 1.73$ ,  $q_0^{(5)}/k^0 = -0.15$  (propagating toward positive  $x$ ), and  $q_0^{(4)}/k^0 = 0.23$ ,  $q_0^{(4)}/k^0 = -1.85$  (propagating toward negative  $x$ ). The agreement here is despite the analytical approximations that were used to derive the dispersion relations in Eq. (32) being expected to be less accurate with the parameters in case IV in Table I, as discussed regarding Fig. 3.

As opposed to the results shown in Fig. 7, where the excitation is due to an impinging plane wave, in Fig. 8 we show some simulation results for excitation by a localized two-dimensional point source; namely, an infinite current line source with uniform amplitude and phase. The source is located near the origin at  $(x_s, y_s) = (a/2, b/2)$ . The other parameters and array dimensions are as assumed

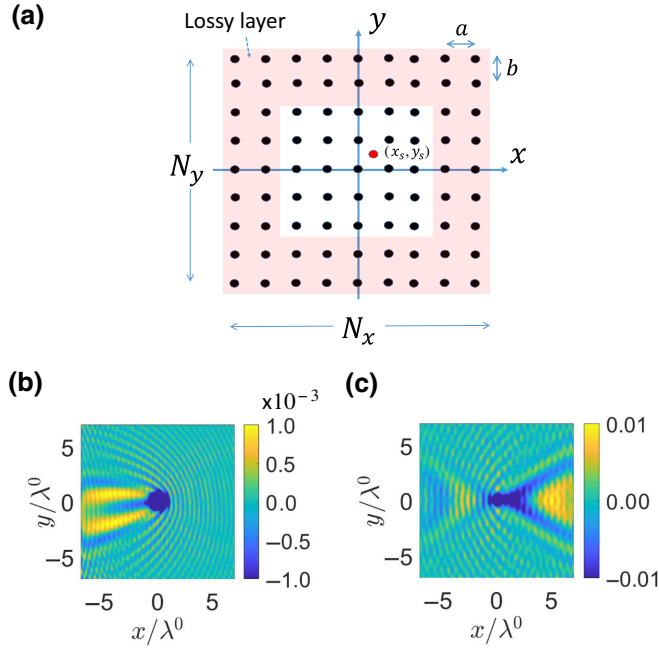


FIG. 8. (a) Illustration of the structure. A current line source, with uniform amplitude and phase, oscillates at  $\delta\omega = -0.15\omega^0$  and is located near the origin, along the  $z$  axis. The current line excites a finite array with  $N_x = 201, N_y = 141$  denoting the number of wires along  $x$  and  $y$ , as in Fig. 7. The remaining parameters are as given in cases III and IV in Table I, and are used in the simulations for the dispersion diagrams of the infinite lattice. (b) For case III, the excited current wave at the source frequency is shown, revealing substantial Fresnel drag, remarkably, already at the fundamental excitation harmonic with low modulation index and frequency. (c) As in (b) but for case IV in Table I.

in the context of Fig. 7. The structure is illustrated in Fig. 8(a). Figures 8(b) and 8(c) we show the excited current waves for the parameters in cases III and IV in Table I, respectively. The calculation is performed by the same method as used before for the plane-wave case, but with a different field source (here the external field is simply considered as that of an infinite current wire at  $\delta\omega = -0.15\omega^0$ ). Figures 8(b) and 8(c) show the current normalized with respect to the maximal excited-current amplitude. In Figs. 8(b) and 8(c) a substantial Fresnel drag is evident, as can be concluded from the highly anisotropic wave picture already at the fundamental source harmonic.

## VII. ARE HOMOGENIZATION AND SPATIOTEMPORAL MODULATION INTERCHANGEABLE OPERATIONS?

In the previous sections we homogenized and derived the effective permittivity of the various modal solutions that are supported by the spatiotemporally modulated wire medium. However, we could also first homogenize the stationary wire medium, leading to its famous plasmalike

behavior, and then introduce the spatiotemporal modulation on the effective properties of the homogenized material. Evidently, the latter approach is expected to be less accurate since it does not take into account the microscopic properties of the modulation; however, it is surely easier to perform. In this section we compare the two approaches. Specifically, near the resonance frequency, the effective permittivity of a stationary wire medium takes the plasmalike form

$$\varepsilon_r = 1 - \frac{\omega_p^2}{\omega^2}. \quad (49)$$

The spatiotemporal modulation of the structure may now be introduced in the effective permittivity parameter  $\omega_p$ .

To be able to perform a fair comparison, it is essential to define the analog of the capacitance modulation discussed in the previous sections. Clearly, in the homogenized model, the only quantity we may modulate is  $\omega_p$ , but then we need to ask for a given capacitance modulation  $\delta C$  in Eq. (10) what the equivalent measure of modulation in  $\omega_p$  is.

To that end, we may estimate the behavior for a small change in  $\omega_p$  and the frequency. Recall that in Sec. IV we defined the frequency that nullifies the effective permittivity of the loaded, but stationary, wire medium as  $\omega^0$  [see Eq. (26)]. In the continuous model that we consider here in Eq. (49),  $\omega_p$  takes the role of  $\omega^0$ . To estimate the small-variation behavior of Eq. (49), we denote  $\omega_p = \omega^0 + \delta\omega_p$  and  $\omega = \omega^0 + \delta\omega$ . Then, for frequencies near the plasma frequency, and for small variations in the plasma frequency, Eq. (49) becomes

$$\varepsilon_r \approx 2 \left( \frac{\delta\omega}{\omega^0} - \frac{\delta\omega_p}{\omega^0} \right). \quad (50)$$

By performing a similar procedure for the effective permittivity of the stationary wire medium that is given in Eq. (8) and comparing the permittivity near the plasma frequency, we find that a variation in  $\omega_p$  is related to a variation in  $C$  via

$$\frac{\delta\omega_p}{\omega^0} = -\frac{\psi}{2} \frac{\delta C}{C_0} \quad (51)$$

when  $\psi \ll 1$ . If  $\psi \gtrsim 1$ , then the simple local plasma model in Eq. (49) is inadequate to describe the effective model of the loaded wire medium. Let us now time-modulate the plasma frequency:

$$\omega_p(\vec{r}, t) = \omega^0 + \delta\omega_p \cos(\Omega t - \varphi), \quad (52)$$

with  $\varphi = \vec{\zeta} \cdot \vec{R}$  and  $\vec{R} = x\hat{x} + y\hat{y}$ . We approximate

$$\omega_p^2(\vec{r}, t) \approx (\omega^0)^2 \left( 1 + 2 \frac{\delta\omega_p}{\omega^0} \cos(\Omega t - \varphi) \right). \quad (53)$$

We assume a  $\hat{z}$ -polarized electric field as in the original wire system. We write Faraday's law in the frequency domain  $\vec{\nabla} \times \vec{H}(\omega) = j\omega\hat{z}\varepsilon(\omega)E(\omega)$  and perform conversion to the time domain ( $1/j\omega \mapsto$  integration):

$$\vec{\nabla} \times \vec{H}(t) = \hat{z}\varepsilon_0 \frac{\partial E(t)}{\partial t} + \hat{z}\varepsilon_0\omega_p^2(t) \int_{-\infty}^t E(\tau) d\tau. \quad (54)$$

We can now return to the frequency domain:

$$\begin{aligned} \vec{\nabla} \times \vec{H}(\omega) &= j\hat{z}\omega\varepsilon_0\vec{E}(\omega) + \hat{z}\varepsilon_0(\omega^0)^2 \\ &\times \left( \delta(\omega) + \frac{\delta\omega_p}{\omega^0} [e^{j\varphi}\delta(\omega - \Omega) \right. \\ &\left. + e^{-j\varphi}\delta(\omega + \Omega)] \right) * \frac{E(\omega)}{j\omega}, \end{aligned} \quad (55)$$

where  $*$  denotes convolution. We derive the equation for the  $n$ th frequency harmonics, and also use the known identity for plane waves  $\vec{\nabla} = -j\vec{q}$ :

$$\begin{aligned} -\frac{1}{\varepsilon_0} j\vec{q} \times \vec{H}_n &= \left( \omega_n - \frac{(\omega^0)^2}{\omega_n} \right) \hat{z}jE_n + \hat{z} \frac{\omega^0\delta\omega_p e^{j\varphi} E_{n-1}}{j\omega_{n-1}} \\ &+ \hat{z} \frac{\omega^0\delta\omega_p e^{-j\varphi} E_{n+1}}{j\omega_{n+1}}. \end{aligned} \quad (56)$$

Using in addition Faraday's equation, we obtain

$$q^2 E_z = -j\omega_n \mu \varepsilon_0 \frac{(-j\vec{q})}{\varepsilon_0} \times \vec{H}. \quad (57)$$

We now get an equation for the electric field, which can be written as an infinite tridiagonal matrix. We now focus on the case of linear phase  $\varphi = \vec{\zeta} \cdot \vec{R}$ .

$$a_{n-1} e^{j\varphi} E_{n-1} - b_n E_n + a_{n+1} e^{-j\varphi} E_{n+1} = 0, \quad (58)$$

with

$$a_n = \frac{k_0 \delta\omega_p}{k_n \omega^0}, \quad (59a)$$

$$b_n = \frac{k_n}{k^0} - \frac{k^0}{k_n} - \frac{q_n^2}{k^0 k_n}. \quad (59b)$$

By our assuming, as in previous sections, that only the three fundamental harmonics are dominant, the recursive relation in Eq. (58) may be truncated, yielding a  $3 \times 3$  homogeneous system for  $E_n$ , with  $n = -1, 0, 1$ . Then, to get a nontrivial solution, we require that its determinant vanishes, yielding

$$\left( \frac{\delta\omega_p}{\omega^0} \right) \left( \frac{a_{-1}}{b_{-1}} + \frac{a_1}{b_1} \right) = b_0, \quad (60)$$

in a way similar to which Eq. (28) was derived. Later, we use Eq. (17) and get the dispersion equation for the various wave solutions supported by the system. For brevity, we omit the expressions; nevertheless, these solutions are then used to calculate the effective permittivity of the various modes, as done in Sec. V. These read

$$\varepsilon_{r;1} = \varepsilon_{r;2} = \frac{[2 + (\delta\omega/\omega^0) - (\delta\hat{\omega}/\omega^0)] [(\delta\omega/\omega^0) - (\delta\hat{\omega}/\omega^0)]}{[1 + (\delta\omega/\omega^0)]^2}, \quad (61a)$$

$$\varepsilon_{r;3,4} = \frac{1}{[1 + (\delta\omega/\omega^0)]^2} \left[ -\frac{\zeta}{k^0} \cos \gamma \pm \frac{k_1}{k^0} \sqrt{-\left(\frac{\zeta}{k_1}\right)^2 \sin^2 \gamma + 1 - \frac{k^0}{k_1}} \right]^2, \quad (61b)$$

$$\varepsilon_{r;5,6} = \frac{1}{[1 + (\delta\omega/\omega^0)]^2} \left[ \frac{\zeta}{k^0} \cos \gamma \pm \frac{k_1}{k^0} \sqrt{-\left(\frac{\zeta}{k_1}\right)^2 \sin^2 \gamma + 1 - \frac{k^0}{k_1}} \right]^2. \quad (61c)$$

For comparison with the effective permittivity that is obtained by directly our homogenizing the spatiotemporally modulated wire medium, we use the transform  $\delta\omega_p/\omega^0 = -(\psi/2)(\delta C/C_0)$  for the cases listed in Table I, and thus get a new set of four corresponding cases, as listed in Table II, where here the modulation depth  $m = \delta\omega_0/\omega^0$ . Specifically, we calculate the effective permittivities for the

modal solutions that correspond to cases II and III. These are shown in Figs. 9 and 10, and should be compared with the wire-medium counterparts in Figs. 5 and 6. Specifically, it is seen that the two homogenization approaches are nearly equivalent, with minor differences for cases with  $\psi \ll 1$ , as seen, for example, by comparing Figs. 9 and 5. This behavior changes for cases with larger capacitive

TABLE II. Four parameter cases used in the numerical examples for the effective permittivity in a continuous plasma model with spatiotemporally modulated plasma-frequency. The values here correspond to these in Table I for the wire medium.

	$m = \delta\omega_p/\omega^0$	$\Omega/\omega^0$	$\zeta/k^0$	$\theta_0$	$\xi$
Case I	0.014	0.15	0.1	$\pi/3$	0
Case II	0.035	0.2	1.0	0	0
Case III	0.03	0.25	1.2	$\pi/5$	$\pi/4$
Case IV	0.18	0.3	1.0	$\pi$	0

loading  $\psi \gtrsim 1$  as seen, for example, by comparing Fig. 10 and 6. In this case, since the capacitive loading is not negligible, the plasma model in Eq. (49) becomes less accurate already for the stationary-medium case [38]. Nevertheless, while the effect of the spatiotemporal modulation on the fundamental solutions No. 1 and No. 2 is moderate, the effect on the higher-order solutions, which dominate below  $\omega^0$ , is substantial, even though the modulation index in this case,  $m = 0.03$ , is small.

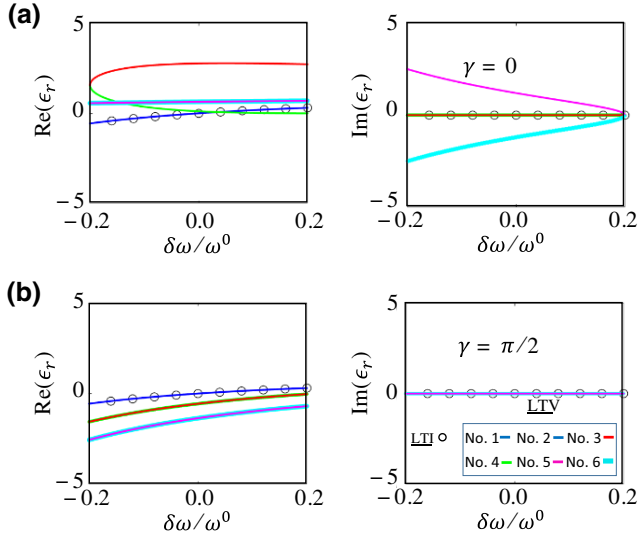


FIG. 9. Effective permittivity of the modal solutions in a spatiotemporally modulated continuous plasmalike model. Results for case II in Table II. This figure should be compared with Fig. 5, which is calculated by brute-force homogenization of the spatiotemporally modulated wire medium. (a) Effective permittivity when the propagation is collinear with the modulation. Circles represent no modulation (stationary plasma medium). Fundamental modal solutions No. 1,2 (continuous blue lines) are nearly identical to these of the stationary medium, and are reciprocal. The higher-order solutions No. 3,4 and No. 5,6 exhibit deviation with respect to the stationary-medium solutions and nonreciprocally. (b) is as (a) but for propagation normal to the direction of modulation. The solutions are reciprocal in this case, and thus the strong anisotropy due to the spatiotemporal modulation clearly emerges from comparison of (a),(b). A comparison with Fig. 5 demonstrates strong similarities between the results of the two homogenization approaches. LTV, linear time variant.

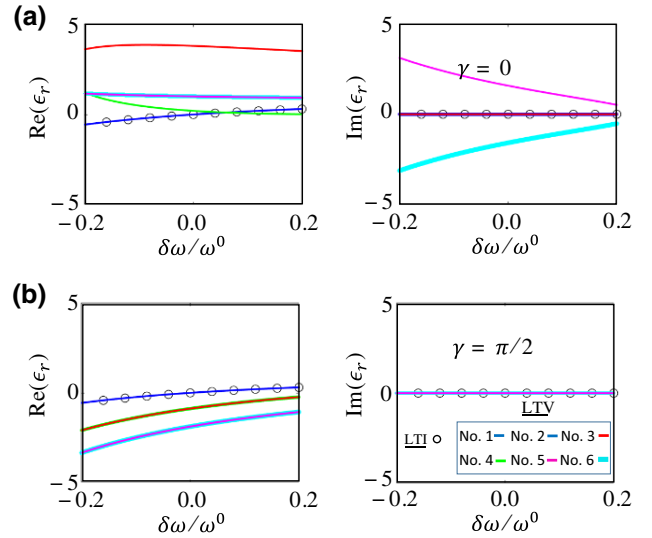


FIG. 10. Effective permittivity in a spatiotemporally modulated continuous plasmalike model. As in Fig. 9 but calculated for case III in Table II. These results should be compared with those in Fig. 6, exhibiting large differences between the two homogenization approaches in the case  $\psi \sim 1$ . LTV, linear time variant.

## VIII. CONCLUSIONS AND OUTLOOK

In this paper we develop a homogenization theory for a spatiotemporally modulated wire medium. Our analysis takes into account the complete interaction between the time-modulated wires, in both space and time. The dispersion relations that we derive for the modes that are supported by the lattice demonstrate peculiar wave phenomena, such as guidance below the cutoff frequency (so-called plasma frequency) of the stationary medium, with modulation depth as weak as desired. This behavior shares similarities with the extraordinary mode that is guided in magnetized plasma, parallel to the magnetization direction, the so-called whistler mode. Furthermore, in light of the ability to guide waves below the plasma frequency, we show that this system provides a means to achieve substantial effective Fresnel drag with weak and slow spatiotemporal modulation. In addition to these wave phenomena, we calculate, analytically, the effective permittivity of the first low-order solutions, and moreover derive expressions for the averaged (macroscopic) fields and the Poynting vector. To verify our dispersion results, and to gain further physical insight regarding the wave dynamics in the structure, we also explore numerically the excitation problem of a finite sample of a spatiotemporally modulated wire medium under plane-wave and point-source excitation. Lastly, we compare the two homogenization approaches for a spatiotemporally modulated wire medium: the first considers the modulation in the homogenization by taking into account the microscopic interactions between the

time-modulated meta-atoms, and second introduces artificially the modulation into the effective parameters of the already homogenized, corresponding stationary medium. We show that under certain conditions these approaches may provide similar results; however, in the general case they may substantially deviate. To conclude, we hope that this work will provide insights regarding the practical realizations of spatiotemporally modulated and time-modulated effective media for various possible applications. This work is a first step in this direction. Subsequent work should consider, among other things, the practical problem of spatiotemporally modulated finite wire media, the interplay between the inherent general nonlocality of stationary wire media for non-TEM propagation, and the nonlocality that is caused by the spatiotemporal modulation. In addition, the development of an excitation theory for spatiotemporally modulated wire media that can predict the complete spectra that should be expected upon excitation, as well as the excitation amplitude, is also called for.

### ACKNOWLEDGMENT

This research was supported by the Israel Science Foundation (Grant No. 1353/19).

### APPENDIX A: EVALUATION OF THE DISPERSION OF A LTI WIRE MEDIUM

This calculation can be found entirely in textbooks, such as in Ref. [38]. Nevertheless, for completeness, we briefly provide it below. The local field at the reference point  $m = l = 0$ ,

$$\begin{aligned} E_z^{\text{loc}} &= -\frac{\eta k I_0}{4} \sum_{m,l \neq 0} H_0^{(2)}(kR_{ml}) e^{-j(q_x am + q_y bl)} \\ &= -\frac{\eta k I_0}{2} \left( S_0 + \sum_{m \neq 0} S_m e^{-j q_x am} \right), \end{aligned} \quad (\text{A1})$$

where  $S_m$  denotes the summation for fixed  $m$ , over the indices  $l$ . For  $m = 0$  we have

$$\begin{aligned} S_0 &= \sum_{l=1}^{\infty} H_0^{(2)}(kR_{0l}) \cos q_y bl \\ &= \frac{1}{b\sqrt{k^2 - q_y^2}} - \frac{1}{2} \\ &\quad + \frac{j}{\pi} \left[ \ln \frac{bk}{4\pi} + \gamma + \frac{1}{2} \sum_{l \neq 0} \left( \frac{-2\pi j}{b\beta_{x,l}} - \frac{1}{|l|} \right) \right]. \end{aligned} \quad (\text{A2})$$

Here  $\gamma = 0.5772$  is the Euler constant. For  $m \neq 0$  we use the Poisson summation, which is highly efficient for a

dense grid, and get

$$\begin{aligned} S_m &= \frac{1}{2} \sum_{l=-\infty}^{\infty} H_0^{(2)}(kR_{ml}) e^{-j q_y bl} \\ &= -\frac{1}{b} \sum_{l=-\infty}^{\infty} \frac{e^{-j a |m| \beta_{x,l}}}{\beta_{x,l}}. \end{aligned} \quad (\text{A3})$$

By substituting Eq. (5b) into Eq. (4), changing the order of summations, and using

$$\sum_{m \neq 0} e^{-j(\beta_{x,l} |m| + q_x am)} = \frac{j \sin \beta_{x,l} a}{\cos \beta_{x,l} a - \cos q_x a} - 1, \quad (\text{A4})$$

we can rewrite Eq. (3):

$$\begin{aligned} &\frac{\eta k}{4} H_0^{(2)}(kr_0) + \frac{1}{j \omega \tilde{C}_0} \\ &= -\frac{\eta k}{2} \left[ S_0 + \sum_{l=-\infty}^{\infty} \frac{1}{\beta_{x,l}} \left( \frac{j \sin \beta_{x,l} a}{\cos \beta_{x,l} a - \cos q_x a} - 1 \right) \right]. \end{aligned} \quad (\text{A5})$$

Note that we assume small losses in the background medium, so convergence is secured. We assume that the wire radius is very small compared with the separation between the wires, and use the approximation for the Hankel function [52]:

$$H_0^{(2)}(kr_0) \approx 1 - j \frac{2}{\pi} \left( \ln \frac{kr_0}{2} + \gamma \right). \quad (\text{A6})$$

This leads to the dispersion relation

$$\begin{aligned} &\frac{j}{\pi} \ln \frac{kr_0}{2} - \frac{2}{jk\eta\omega\tilde{C}_0} \\ &= \frac{1}{b\sqrt{k^2 - q_y^2}} + \frac{j}{\pi} \left[ \ln \frac{bk}{4\pi} + \frac{1}{2} \sum_{l \neq 0} \left( \frac{-2\pi j}{b\beta_{x,l}} - \frac{1}{|l|} \right) \right] \\ &\quad + \sum_{l=-\infty}^{\infty} \frac{1}{\beta_{x,l}} \left( \frac{j \sin \beta_{x,l} a}{\cos \beta_{x,l} a - \cos q_x a} - 1 \right). \end{aligned} \quad (\text{A7})$$

For a dense grid ( $ka, kb \ll 1$ ), with the approximations for trigonometric functions with small arguments, we get

$$\begin{aligned} &\ln \frac{b}{2\pi r_0} + \sum_{l=1}^{\infty} \frac{\coth(\pi a l/b) - 1}{l} - \frac{2\pi}{\eta v k^2 \tilde{C}_0} \\ &= \frac{2\pi}{ab \left[ k^2 - (q_x^2 + q_y^2) \right]} - \frac{\pi a}{6b}. \end{aligned} \quad (\text{A8})$$



**APPENDIX B: DERIVATION OF EQ. (11)**

We begin by transforming the expression for the frequency-domain susceptibility of a loaded wire, i.e., Eq. (1), into the time-domain expression. It is easy to see that  $\alpha^{-1}$  behaves as an impedance to unit length, and  $E^{\text{loc}}$  behaves as an external “voltage” source (obviously with unit of volts per meter). Therefore, we can consider our physical model to be equivalent to the simple serial circuit that is shown in Fig. 11 with stationary impedance  $\alpha_0^{-1}$  per unit length (involves resistance as well as reactance) and time-modulated capacitance. The current on the capacitor reads

$$I = \frac{d}{dt}(\tilde{C}(t) E_C(t)), \quad (\text{B1})$$

where  $E_C$  denotes the “voltage” on the capacitance. Then, Eq. (11) is straightforward.

**APPENDIX C: DERIVATION OF EQ. (17)**

The wire medium behaves as an infinite periodic crystal, and therefore we can use the Floquet-Bloch theorem, with the expression in Eq. (16). By substituting Eq. (16) into Eq. (15) and using the explicit expression for the phase of the capacitors  $\varphi_{m,l} = \vec{\zeta} \cdot \vec{r} = ma\zeta \cos \xi + bl\zeta \sin \xi$ , we get for the  $m, l$  wire and for  $n$ th mode

$$\begin{aligned} E_n^{\text{inc}} e^{-j\vec{q}_n \cdot \vec{R}_{ml}} &= \left( \gamma_0 \omega_n + \frac{1}{j \omega_n \tilde{C}_0} \right) A_n e^{-j\vec{q}_n \cdot \vec{R}_{ml}} \\ &- A_{n-1} \frac{m}{2} \frac{1}{j \omega_{n-1} \tilde{C}_0} e^{-j(\vec{\zeta} + \vec{q}_{n-1}) \cdot \vec{R}_{ml}} \\ &- A_{n+1} \frac{m}{2} \frac{1}{j \omega_{n+1} \tilde{C}_0} e^{-j(-\vec{\zeta} + \vec{q}_{n+1}) \cdot \vec{R}_{ml}}. \end{aligned} \quad (\text{C1})$$

Equation (C1) must be valid for all  $m, l$  wires. Therefore, we must require that

$$-\vec{\zeta} - \vec{q}_{n-1} = -\vec{q}_n \quad \text{and} \quad \vec{\zeta} - \vec{q}_{n+1} = -\vec{q}_n. \quad (\text{C2})$$

Therefore, we get  $\vec{q}_n = \vec{q}_0 + n\vec{\zeta}$  as in Eq. (17).

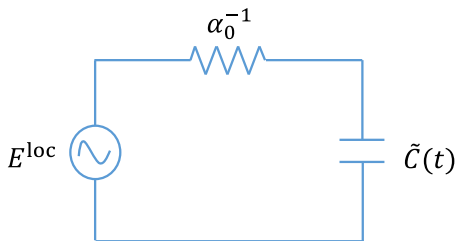


FIG. 11. The equivalent circuit of a wire illuminated by an external field.

**APPENDIX D: CALCULATING THE FIELD IN THE UNIT CELL**

To evaluate the electric field in the unit cell at the origin, we use Eq. (38):

$$\begin{aligned} \vec{E}(\vec{r}) &= -\frac{\hat{z}\eta k I_0}{2b} \sum_{m=-\infty}^{\infty} \\ &\times \sum_{l=-\infty}^{\infty} \frac{e^{jy[q_y + (2\pi l/b)]} e^{-ja|m-(x/a)|\beta_{x,l}} e^{-jq_x a m}}{\beta_{x,l}}. \end{aligned} \quad (\text{D1})$$

Then we approximate  $\beta_{x,l} = -j\sqrt{[q_y + (2\pi l/b)]^2 - k^2} \approx -j[(2\pi l/b) + q_y]$ . This leads to

$$\begin{aligned} \vec{E}(\vec{r}) &= -\frac{\hat{z}\eta k I_0}{2b} \times \sum_{l=-\infty}^{\infty} \frac{e^{jy[q_y + (2\pi l/b)]}}{\beta_{x,l}} \\ &\times \left( \frac{e^{-j(a+x)\beta_{x,l}} e^{jq_x a}}{1 - e^{-ja\beta_{x,l}} e^{jq_x a}} + e^{-j|x|\beta_{x,l}} \right. \\ &\left. + \frac{e^{-j(a-x)\beta_{x,l}} e^{-jq_x a}}{1 - e^{-ja\beta_{x,l}} e^{-jq_x a}} \right). \end{aligned} \quad (\text{D2})$$

For a dense grid,  $\beta_{x,l}$  may be further approximated:

$$\beta_{x,l} \approx \begin{cases} \sqrt{k^2 - q_y^2}, & l = 0, \\ -j\left(\frac{2\pi|l|}{b} + q_y\right), & l \neq 0. \end{cases} \quad (\text{D3})$$

We can see that we get  $\beta_{x,l} \approx \beta_{x,-l}$ . This eventually leads to Eq. (40).

**APPENDIX E: VERY-DENSE GRID**

We compare Eq. (44) with the average over the  $z$  component of the electric field as calculated in Ref. [22]:

$$\langle E_z \rangle = (j\omega\tilde{L} + Z_w)I + \frac{\partial\varphi}{\partial z}, \quad (\text{E1})$$

where  $\tilde{L}$  is the effective inductance per unit length of the wire and  $Z_w$  is the impedance loading on the wire. In our case, for a perfect-electric-conductor wire with capacitance load, we have  $Z_w = 1/j\omega\tilde{C}_0$ . Also, since we are focusing on the case of a propagating wave in a direction normal to the wires, there is no variation along the  $z$  axis and thus we can nullify the potential derivative  $\partial\varphi/\partial z = 0$ .

Then we get

$$\begin{aligned} \langle E_z \rangle &= jI \left[ \left( 1 + \frac{\delta\omega}{\omega^0} \right) \omega^0 \tilde{L} - \frac{1}{[1 + (\delta\omega/\omega^0)] \omega^0 \tilde{C}_0} \right] \\ &\approx jI \frac{\eta}{abk^0} \left[ 1 + (1 + 2\psi) \left( \frac{\delta\omega}{\omega^0} \right) \right]. \end{aligned} \quad (\text{E2})$$

Equation (E2) is valid for a very-dense grid in a stationary medium. Now to show that our averaged field in Eq. (44) is consistent with that, the second term in Eq. (44) should be ignored for a very-dense grid. Then, using Eq. (31) for the wave number in the media (with zero perturbation  $\delta C = 0$ ), we get

$$\begin{aligned} \langle \vec{E} \rangle &\approx -\frac{\hat{z}\eta k_0 I}{ab} \left( \frac{1}{j(k_0^2 - q_0^2)} \right) \\ &\approx -\frac{\hat{z}\eta k_0 I}{ab} \left( \frac{1}{j \left( k_0^2 - (k^0)^2 [1 + (\delta\omega/\omega^0)]^2 \left[ 1 - \frac{1}{[1 + (\delta\omega/\omega^0)]^2 (1 + \psi) - \psi} \right] \right)} \right) \\ &\approx j \frac{\hat{z}\eta I}{abk^0} \left( \frac{1 + (\delta\omega/\omega^0)}{1 + 2(\delta\omega/\omega^0) - 2(1 + \psi)(\delta\omega/\omega^0)} \right) \\ &\approx j \frac{\hat{z}\eta I}{abk^0} \left( 1 + (1 + 2\psi) \frac{\delta\omega}{\omega^0} \right). \end{aligned} \quad (\text{E3})$$

Identical to Eq. (E2).

- 
- [1] R. L. Fante, Transmission of electromagnetic waves into time-varying media, *IEEE Trans. Antennas Propag.* **193**, 417 (1971).
- [2] F. R. Morgenthaler, Velocity modulation of electromagnetic waves, *IRE Trans. Microw. Theory Tech.* **6**, 167 (1958).
- [3] A. Akbarzadeh, N. Chamanara, and C. Caloz, Inverse prism based on temporal discontinuity and spatial dispersion, *Opt. Lett.* **43**, 3297 (2018).
- [4] S. F. Preble, Q. Xu, and M. Lipson, Changing the colour of light in a silicon resonator, *Nat. Photonics* **1**, 293 (2007).
- [5] Daniel Torrent, Olivier Poncelet, and Jean-Christophe Batsale, Nonreciprocal Thermal Material by Spatiotemporal Modulation, *Phys. Rev. Lett.* **120**, 125501 (2018).
- [6] H. Nassar, X. C. Xu, A. N. Norris, and G. L. Huang, Modulated phononic crystals: Non-reciprocal wave propagation and Willis materials, *J. Mech. Phys. Sol.* **101**, 10 (2017).
- [7] N. A. Estep, D. L. Sounas, J. C. Soric, and A. Alú, Magnetic-free non-reciprocity and isolation based on parametrically modulated coupled-resonator loops, *Nat. Phys.* **10**, 923 (2014).
- [8] J. R. Zurita-Sánchez, P. Halevi, and J. C. Cervantes-González, Reflection and transmission of a wave incident on a slab with a time-periodic dielectric function, *Phys. Rev. A* **79**, 053821 (2009).
- [9] J. S. Martínez-Romero, O. M. Becerra-Fuentes, and P. Halevi, Temporal photonic crystals with modulations of both permittivity and permeability, *Phys. Rev. A* **93**, 063813 (2016).
- [10] V. Bacot, M. Labousse, A. Eddi, M. Fink, and E. Fort, Time reversal and holography with spacetime transformations, *Nat. Phys.* **12**, 972 (2016).
- [11] S. Vezzoli, V. Bruno, C. DeVault, T. Roger, V. M. Shalaev, A. Boltasseva, M. Ferrera, M. Clerici, A. Dubietis, and D. Faccio, Optical Time Reversal from Time-Dependent Epsilon-Near-Zero Media, *Phys. Rev. Lett.* **120**, 043902 (2018).
- [12] M. A. Salem and C. Caloz, in *9th European Conference on Antennas and Propagation (EuCAP)* (IEEE, Piscataway, NJ, 2015), p. 2164.
- [13] M. A. Salem and C. Caloz, in *International Conference on Electromagnetics in Advanced Applications (ICEAA)* (IEEE, Torino, 2015).
- [14] G. Lerosey, J. De Rosny, A. Tourin, A. Derode, G. Montaldo, and M. Fink, Time Reversal of Electromagnetic Waves, *Phys. Rev. Lett.* **92**, 193904 (2004).
- [15] V. Pacheco-Peña, Effective medium concept in temporal metamaterials, *Nanophotonics* **9**, 379 (2020).
- [16] D. M. Solis and N. Engheta, A generalization of the Kramers-Kronig relations for linear time-varying media, *Phys. Rev. B* **103**, 144303 (2021).
- [17] Y. Hadad, D. L. Sounas, and A. Alú, Space-time gradient metasurfaces, *Phys. Rev. B* **92**, 100304(R) (2015).
- [18] Y. Hadad, J. C. Soric, and A. Alú, Breaking temporal symmetries for emission and absorption, *Proc. Natl. Acad. Sci.* **113**, 3471 (2016).

- [19] Y. Hadad and D. L. Sounas, Space-time modulated loaded-wire metagratings for magnetless nonreciprocity and near-complete frequency conversion, [arXiv:1906.00215](https://arxiv.org/abs/1906.00215) (2019).
- [20] A. Shlivinski and Y. Hadad, Beyond the Bode-Fano Bound: Wideband Impedance Matching for Short Pulses Using Temporal Switching of Transmission-Line Parameters, *Phys. Rev. Lett.* **121**, 204301 (2018).
- [21] H. Li and A. Alú, Temporal switching to extend the bandwidth of thin absorbers, *Optica* **8**, 24 (2021).
- [22] S. I. Maslovski and M. G. Silveirinha, Nonlocal permittivity from a quasistatic model for a class of wire media, *Phys. Rev. B* **80**, 245101 (2009).
- [23] P. A. Belov, S. A. Tretyakov, and A. J. Viitanen, Dispersion and reflection properties of artificial media formed by regular lattices of ideally conducting wires, *J. Electromagn. Waves Appl.* **16**, 1153 (2012).
- [24] N. A. Nicorovich, R. C. McPhedran, and L. C. Botten, Photonic band gaps for array of perfectly conducting cylinders, *Phys. Rev. E* **52**, 1135 (1995).
- [25] S. K. Chin, N. A. Nicorovich, and R. C. McPhedran, Green's function and lattice sums for electromagnetic scattering by a square array of cylinders, *Phys. Rev. E* **49**, 4590 (1994).
- [26] V. Kuzmiak, A. A. Maradudin, and F. Pincemin, Photonic band structures of two dimensional systems containing metallic components, *Phys. Rev. B* **50**, 16835 (1994).
- [27] V. Kuzmiak, A. A. Maradudin, and A. R. McGurn, Photonic band structures of two dimensional systems fabricated from rods of a cubic polar crystal, *Phys. Rev. B* **55**, 4298 (1997).
- [28] K. Sakoda, Photonic bands of metallic systems I. Principle of calculation and accuracy, *Phys. Rev. B* **64**, 045116 (2001).
- [29] M. M. Sigalas, Metallic photonic band gap materials, *Phys. Rev. B* **52**, 11744 (1995).
- [30] M. G. Silveirinha and S. I. Maslovski, Radiation from elementary sources in a uniaxial wire medium, *Phys. Rev. B* **85**, 155125 (2012).
- [31] M. G. Silveirinha, Additional boundary condition for the wire medium, *IEEE Trans. Antennas Propag.* **54**, 1766 (2006).
- [32] M. G. Silveirinha, C. A. Fernandes, and J. R. Costa, Additional boundary condition for a wire medium connected to a metallic surface, *New J. Phys.* **10**, 053011 (2008).
- [33] M. G. Silveirinha, C. A. Fernandes, and J. R. Costa, Electromagnetic characterization of textured surfaces formed by metallic pins, *IEEE Trans. Antennas Propag.* **56**, 405 (2008).
- [34] G. W. Hanson, E. Forati, and M. G. Silveirinha, Modeling of spatially-dispersive wire media: Transport representation, comparison with natural materials, and additional boundary conditions, *IEEE Trans. Antennas Propag.* **60**, 4219 (2012).
- [35] E. Forati and G. W. Hanson, Scattering from isotropic connected wire medium metamaterials: Three-, two-, and one-dimensional cases, *IEEE Trans. Antennas Propag.* **61**, 3564 (2013).
- [36] G. W. Hanson, M. G. Silveirinha, P. Burghignoli, and A. B. Yakovlev, Nonlocal susceptibility of the wire medium in the spatial domain considering material boundaries, *New J. Phys.* **15**, 083018 (2013).
- [37] A. B. Yakovlev, M. Hedayati, M. G. Silveirinha, and G. W. Hanson, A local thickness-dependent permittivity model for non-local bounded wire-medium structures, *Phys. Rev. B* **94**, 155442 (2016).
- [38] S. Tretyakov, *Analytical Modeling in Applied Electromagnetics* (Artech House, Boston, 2003).
- [39] A. Ishimaru, *Electromagnetic Wave Propagation, Radiation, and Scattering* (Prentice-Hall, New-Jersey, 1991).
- [40] P. A. Huidobroa, E. Galiffib, S. Guenneau, R. V. Crassterc, and J. B. Pendryb, Fresnel drag in space-time-modulated metamaterials, *Proc. Natl. Acad. Sci.* **116**, 24943 (2019).
- [41] D. M. Solís, R. Kastner, and N. Engheta, Time-varying materials in presence of dispersion: Plane-wave propagation in a Lorentzian medium with temporal discontinuity, [arXiv:2103.06142](https://arxiv.org/abs/2103.06142) (2021).
- [42] D. M. Solís and N. Engheta, Functional analysis of the polarization response in linear time-varying media: A generalization of the Kramers-Kronig relations, *Phys. Rev. B* **103**, 144303 (2021).
- [43] S. I. Maslovski, T. A. Morgado, M. G. Silveirinha, C. S. R. Kaipa, and A. B. Yakovlev, Generalized additional boundary conditions for wire media, *New J. Phys.* **12**, 113047 (2010).
- [44] C. S. R. Kaipa, A. B. Yakovlev, S. I. Maslovski, and M. G. Silveirinha, Indefinite dielectric response and all-angle negative refraction in a structure with deeply-subwavelength inclusions, *Phys. Rev. B* **84**, 165135 (2011).
- [45] O. Rabinovich and A. Epstein, Analytical design of printed circuit board (PCB) metagratings for perfect anomalous reflection, *IEEE Trans. Antennas Propag.* **66**, 4086 (2018).
- [46] C. Firestein, A. Shlivinski, and Y. Hadad, Absorption and scattering by a temporally switched lossy layer: Going beyond the Rozanov bound, [arXiv:2105.01487](https://arxiv.org/abs/2105.01487) (2021).
- [47] R. E. Collin, *Field Theory of Guided Waves* (Oxford University, Wiley, 1991).
- [48] M. S. Mirmoosa, T. T. Koutserimpas, G. A. Ptitsyn, S. A. Tretyakov, and R. Fleury, Dipole polarizability of time-varying particles, [arXiv:2002.12297v2](https://arxiv.org/abs/2002.12297v2) (2020).
- [49] Y. Mazar and A. Alú, Nonreciprocal hyperbolic propagation over moving metasurfaces, *Phys. Rev. B* **99**, 045407 (2019).
- [50] Y. Mazar and A. Alú, One way hyperbolic metasurfaces based on synthetic motion, *IEEE Trans. Antennas Propag.* **68**, 1739 (2020).
- [51] T. Boyd, J. Gratus, P. Kinsler, R. Letizia, and R. Seviour, Mode profile shaping in wire media: Towards an experimental verification, *Appl. Sci.* **8**, 1276 (2018).
- [52] F. W. J. Olver, A. B. Olde Daalhuis, D. W. Lozier, B. I. Schneider, R. F. Boisvert, C. W. Clark, B. R. Miller, B. V. Saunders, H. S. Cohl, and M. A. McClain, in *NIST Handbook of Mathematical Functions* (Cambridge University Press, 2010), <http://dlmf.nist.gov/>.